Università degli Studi di Padova
Dipartimento di Biologia
Corso di Laurea Magistrale in Molecular Biology

Tesi di Laurea

Generation and characterization of plants expressing flavodiiron proteins to increase biomass yield.

Relatore: Prof. Tomas Morosinotto
Dipartimento di Biologia

Laureando: Filippo Fiorin

Anno Accademico 2023/2024

Summary

Abstract

In eukaryotic photosynthetic organisms the excitatory interaction between light and pigments associated with photosystems I and II provides the driving energy for Linear Electron Flow (LEF), culminating in the production of reducing equivalents and in the generation of an electrochemical gradient across thylakoid membranes. To dynamically respond to environmental changes and metabolic requirements, photosynthetic organisms evolved several alternative electron flows like the Cyclic Electron Flow (CEF) and pseudo-Cyclic Electron Flow (pseudo-CEF, or water-water cycle).

Flavodiiron proteins (FLVs) divert electrons coming from PSI to reduce water, and previous studies have demonstrated the role of FLVs in protecting PSI from over-reduction and consequent photodamage upon sudden changes in light intensity in cyanobacteria, green algae and bryophytes.

Despite their biological relevance in many photosynthetic organisms, FLVs are absent in Angiospermae. This opens the possibility that their introduction in crops may serve as an instrument to increase the tolerance to light fluctuations and thus stress tolerance, ultimately improving photosynthetic efficiency.

To test this hypothesis, *flv* genes from the bryophyte *Physcomitrium patens* were successfully expressed in *Nicotiana tabacum* and physiologic parameters were assessed. In addition, transgenic *Solanum lycopersicum* plants expressing FLVs were also obtained.

Data presented in this work suggest that FLVs are functional in Angiospermae, where they are indeed active in protecting PSI from over-reduction in the first instants after sudden increases in light intensity and when grown in fluctuating light conditions.

1. Introduction

Since more than 10 000 years humans have grown plants to feed both the population and livestock as well as to obtain useful byproducts from plant harvesting.
Over time crop yield has drastically increased thanks to a variety of factors, such as the technological improvement of traditional farming methods and the use of fertilizers, pesticides and herbicides.

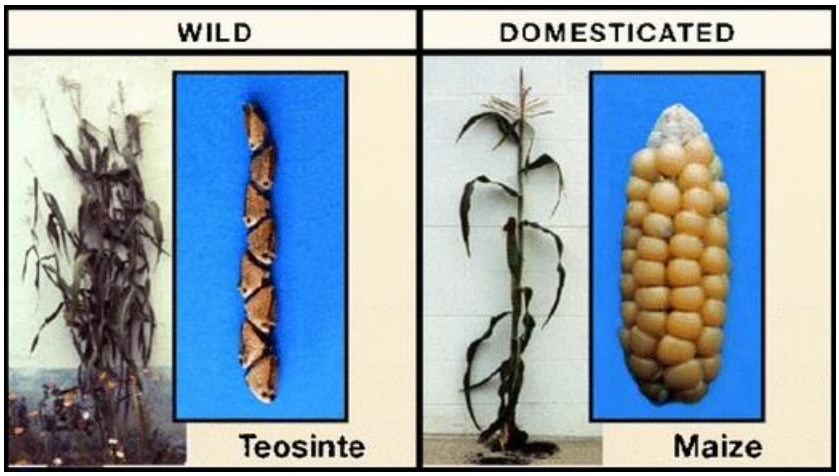

Fig. 1.1 - Comparison between the maize progenitor, Teosinte, and cultivated maize. Enhanced kernel size and gigantism are a result of selective breeding [1].

A major part responsible for the improved productivity is the genetic improvement of the plants obtained by artificial selection of traits that result in enhanced yield. This process of artificial selection of traits started with the beginning of agriculture and resulted in what is commonly known as the "domestication syndrome" which makes currently cultivated plants highly different from their wild ancestors (Fig. 1.1). Depending on the species, the domestication syndrome typically includes phenotypes such as the simultaneous ripening of fruits and seeds, increased fruit biomass and seed size, loss of natural seed dispersal, rapid germination and gigantism [2].

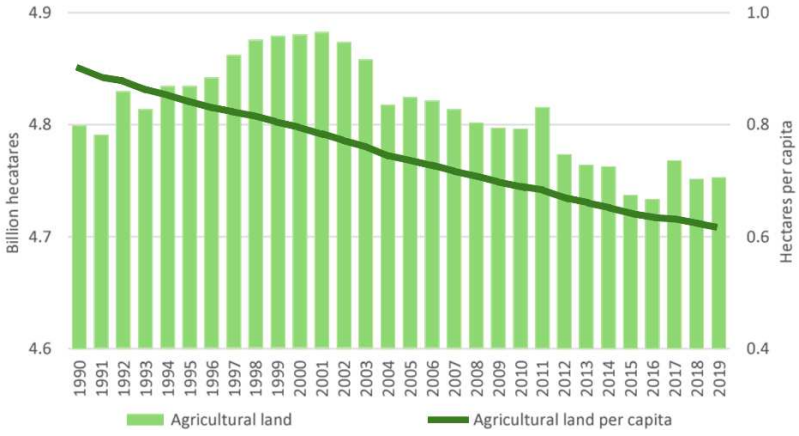

Fig. 1.2 - Absolute and per capita values of global agricultural land between 1990 and 2019 [5].

Increasing crop yield through to selective breeding has proven to be an astonishingly effective approach, but it is intrinsically limited by the resulting erosion of genetic diversity and the resulting uniformity of genotypes [3].
Moreover, while the human population is expected to increase up to 9.8 billion people by 2050 [4], available agricultural land has decreased by 30% since 1990 [5] (Fig. 1.2) creating a need for an additional effort to increase crop yield. One promising possibility which could overcome the limitations of selective breeding may come from genetic engineering.
In the last years agriculture has been the first sector to invest heavily in the use of genetic modifications [6] to create transgenic crop strains (i.e. genetically modified organisms, GMO) with increased stress tolerance or with acquired traits, with the aim of increasing their yield. While the use of GMOs in agriculture raises important questions regarding their biosafety and sustainability, the genetic engineering of crops has unquestionable potential and requires a thorough exploration of the possibilities it offers and of the risks it poses.

The yield of a specific crop in any given region (YP) can be described as:

$$YP = 0.487S_t \times \varepsilon_i \times \varepsilon_c \times \varepsilon_p$$

With $0.487S_t$ being the fraction of the incident solar radiation during growth season that is photosynthetically active, ε_i being the radiation interception efficiency, ε_c being the conversion efficiency of intercepted radiation into biomass and ε_p being the partition of biomass into harvestable products, also called Harvest Index [7] (HI). The conversion efficiency of intercepted radiation into biomass is relatively inefficient in higher plants, with its theoretical maximum being at approximately 5% in most plants and with much lower efficiencies (<1%) observed in the field in temperate climates. While some efficiency losses are unavoidable, because they are caused by optic properties of pigments, there is still room for improvement. The efficiency of the conversion of absorbed light into biomass can be enhanced through genetic engineering with approaches that either improve the efficiency with which carbon is fixed or that improve the efficiency with which light is harvested by plants and converted to chemical energy. One way to achieve this increase in the efficiency of light-driven photosynthetic reactions could consist in the introduction of molecular mechanisms that decrease the amount of damage that the photosynthetic machinery sustains during its functioning [8].

1.1 Photosynthesis

Photosynthesis can be described as a process in which light energy is captured and stored by an organism, and the stored energy is used to drive energy-requiring cellular processes [9].

Indeed, chlorophyll *a*-containing photosynthetic organisms harvest the photosynthetically active radiation (PAR), which is the fraction of the sunlight spectrum from 400 to 700 nanometres, and exploit its converted energy to support the fixation of inorganic carbon into biomass.
This process makes photosynthetic organisms the entry point of inorganic carbon into the biosphere, classifying them as primary producers.
Photosynthesis is an ancient process. The earliest cyanobacteria-like microfossils are dated 3.5 billion years ago, not long after the supposed origin of life, when Earth's atmosphere was still anoxic. Later, 2.7 billion years ago, the Earth was already dominated by photosynthetic cyanobacteria and their photosynthetic activity caused the early surge of atmospheric oxygen concentration [(10)]. Large amounts of evidence suggest that photosynthetic eukaryotes evolved later, as a result of multiple independent endosymbiotic events [(11)] which gave origin to the chloroplasts, around 1.2 billion years ago.
Chloroplasts are double-membrane organelles provided with their own bacteria-like genetic material as well as their own ribosomes. Chloroplasts are also internally sub-compartmentalized in thylakoids, which are membranous structures typically stacked upon one another to form grana. The thylakoid membrane is, in fact, the site of primary light-dependent photosynthetic reactions, which are redox reactions responsible for the early conversion of electromagnetic energy into chemical energy. In plants, the photosynthetic process takes place mainly in the leaf, in mesophyll cells, which are rich in chloroplasts. Each chloroplast is provided with its own inner thylakoid structure where photosynthesis takes place (Fig. 1.4).

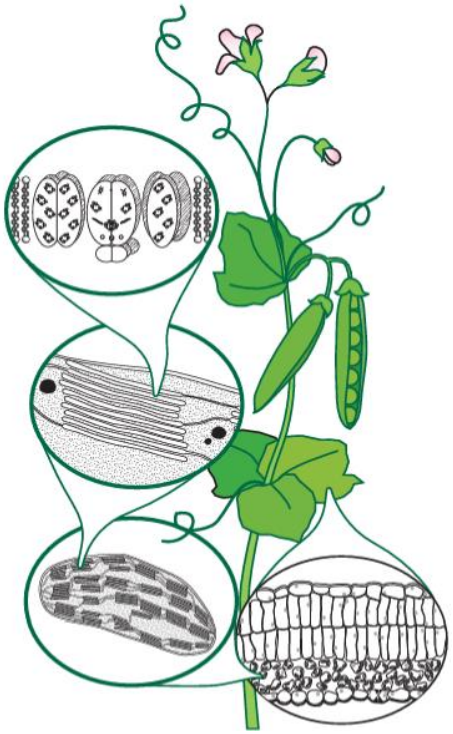

Fig. 1.4 – Schematic diagram of the photosynthetic apparatus of an angiosperm. The leaves of a plant are its photosynthetic organ, whose cells bear a high number of chloroplasts. Each chloroplast is sub-compartmentalized in thylakoids, whose membrane is the site where primary photosynthesis takes place due to the presence of the molecular photosynthetic machinery [(9)].

Photosynthesis has been classically divided into light-dependent and light-independent reactions but, as pointed out by Robert E. Blankenship in *Molecular mechanisms of Photosynthesis*, the only strictly light-dependent process in photosynthesis is photon absorption. Light-dependent photosynthetic reactions can indeed be classified into four processes:

1. Light absorption and delivery to reaction centres
2. Primary electron transfer in reaction centres (charge separation)
3. Energy stabilization by secondary processes
4. Synthesis and export of stable products

The first, light-dependent step of photosynthetic reactions consists in the interaction between a photon and a pigment molecule. Light does not typically interact directly with photosynthetic reaction centres (RCs) but rather with surrounding antenna complexes and with light harvesting complexes (LHCs), which function as antennae that form large arrays around the RCs. This interaction causes the protein-bound pigments to transition from the electronic ground state to an excited state, the singlet state, and the harvested energy is subsequently transferred to the reaction centres through Forster resonance energy transfer [12]. In the absence of biotic and abiotic stresses an efficient harvest of light is an advantage, but under conditions that limit CO_2 fixation (e.g. nutrient depletion, water stress) the absorption of excess light can lead to damage due to the formation of chlorophyll triplet states which cause the formation of ROS. Because of this, both antenna systems and reaction centres display a high number of photo-protecting mechanisms that either dissipate excess energy or divert excess electrons.

Reaction centres are the sites where harvested electromagnetic energy converges in order for primary charge separation to occur, and antenna complexes are involved in the harvesting of light. Together, these two components constitute a photosystem [13]. Despite differences in primary sequence PSII and PSI are similarly structured around their RCs, which are formed by a special pair of chlorophyll molecules.
PSII is structured so that the inner antenna complexes CP43 and CP47 are located on both sides of the D1-D2 heterodimer, in which the P_{680} reaction centre is located along with the primary electron acceptor pheophytin (Pheo). In PSI, instead, the PsaA and PsaB subunits form both the inner antenna complexes and coordinate the reaction centre P_{700} along with subsequent electron acceptors A_0, A_1 and Fx [12]. When the reaction centre of either PSII or PSI receives energy (likely from antenna complexes but also through direct excitation) the chlorophyll molecules therein transition from the electronic ground state to an excited state, which has lower redox potential (E_m) and is thus a reducing species. Because of this, the excited P_{680} or P_{700} gain the ability to reduce the primary electron acceptors, which are Pheo and A_0, respectively, thus performing charge separation. To avoid the reverse reaction in which the

reduced primary electron acceptor donates the electron back to the reaction centre (charge recombination) a series of fast sequential redox reaction occur within the photosystems to physically separate the reduced species from the oxidized reaction centre.
Once stable charge separation is achieved, the electrons from either of the two photosystems are sequentially transferred in an electron transport chain (Fig. 1.5).

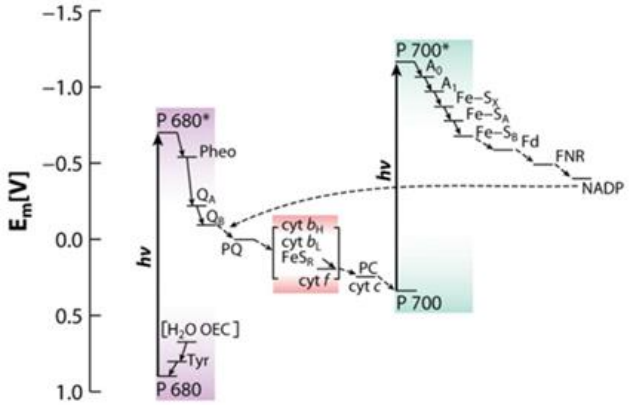

Fig. 1.5 – Schematic representation of the linear electron transport chain of oxygen evolving photosynthetic organisms[9].

In plants the two photosystems, PSII and PSI, work in series and the main electron transport chain develops linearly between them, defining the linear electron flow (LEF). The final electron acceptor of PSII is a molecule of plastoquinone (PQ), which accepts two electrons to be reduced to plastoquinol (PQH_2). The oxidised P_{680}^+ is the strongest known oxidant in biology, and it is restored by the activity of the oxygen evolving complex (OEC), which oxidizes water into oxygen and exploits the resulting electrons to reduce the reaction centre, also providing protons that contribute to the formation of an electrochemical proton gradient across the thylakoid membrane.
Downstream of PSII, plastoquinol acts as an electron donor for the Cytochrome b_6f complex (Cyt b_6f), where it enters the electron bifurcation mechanism called the plastoquinone cycle. Thanks to this process, Cyt b_6f is able to exploit the electrons that result from the oxidation of plastoquinol to reduce both plastoquinone and plastocyanin (PC). The PQ cycle also contributes to the formation of the electrochemical proton gradient across the thylakoid membrane as it releases two protons in each half-cycle [(14)].
Plastocyanin is a copper-containing protein localized in the thylakoid lumen, and once reduced it acts as the electron donor for the oxidized reaction centre of PSI, P_{700}^+. Once charge separation happens in the RC of PSI, the donated electron is transferred between chlorophyll molecules (A_0 and A_1) and sulphur clusters towards the final electron acceptor of PSI, ferredoxin (Fdx).
Fdx is a small soluble protein that acts as electron acceptor for PSI and can reduce a high number of targets. As part of the photosynthetic linear electron flow, Fdx acts as the substrate of the ferredoxin-$NADP^+$ reductase (FNR) in order to reduce $NADP^+$ into NADPH, but Fdx is actually able to reduce various

ferredoxin-dependent enzymes involved in many physiological processes [15]. Thanks to this, Fdx regulates the enzymatic activity of the chloroplast according to photosynthesis and, in particular, it controls the activity of enzymes involved in carbon fixation. Overall, the photosynthetic linear electron flow from water to $NADP^+$ is responsible for the generation NADPH, which is a fundamental energy-carrying cofactor in many metabolic processes, and for the generation of the electrochemical proton gradient across the thylakoid membrane that drives ATP synthesis through the ATP synthase (Fig. 1.6).

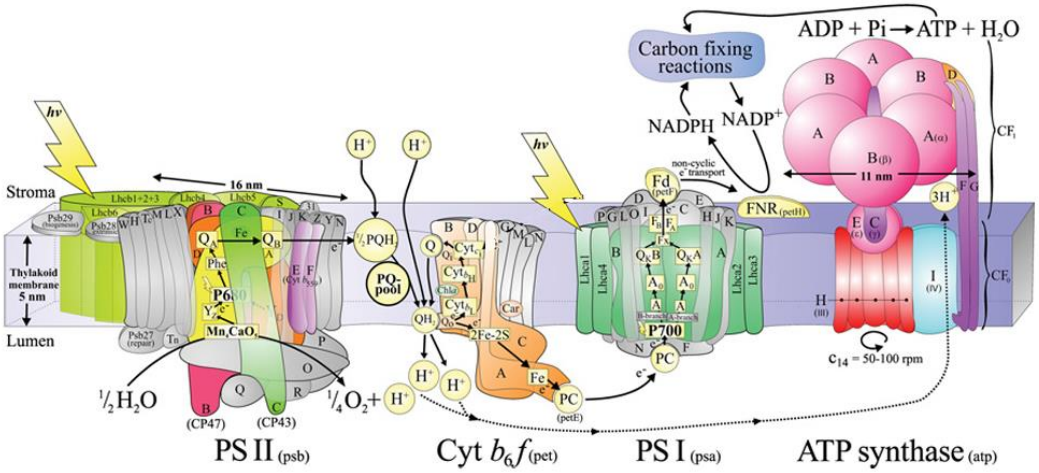

Fig. 1.6 – Figure showing the major protein complexes involved in the photosynthetic linear electron flow and the electron path. Adapted from [9].

Canonically, light-independent photosynthetic reactions are those that exploit reducing equivalents and ATP produced by the photosynthetic electron flow to fix inorganic carbon, which is a process correctly described by the Calvin-Benson-Bassham cycle (CBB). The CBB cycle is carried out by enzymes located in the stromal region of the chloroplast and it can be divided into three phases: carboxylation, reduction and regeneration.

The carboxylation phase consists of the carboxylation of 3 ribulose 1,5-bisphosphate molecules, it is catalysed by the Rubisco enzyme, and it produces 6 molecules of 3-phosphoglycerate. This carboxylation reaction is the entry point of inorganic carbon in the biosphere, a fundamental step in the carbon biogeochemical cycle which converts 100 gigatons of carbon into biomass annually. Rubisco is an esadecameric protein formed by 8 large subunits and 8 small subunits encoded by the nuclear genome; it evolved approximately 3 billion years ago in an oxygen-poor atmosphere and is characterized by its capability to react with both CO_2 and O_2. The off-target oxygenation of ribulose 1,5-bisphosphate results in the production of 2-phosphoglycolate instead of 3-phosphoglycerate, with the former that must be recycled in a process called photorespiration.

Once the 3-phosphoglycerate molecules have been produced they undergo the second phase of the CBB cycle – the reduction – which exploits 6 molecules of

ATP and 6 molecules of NADPH to phosphorylate and reduce six molecules of 3-phosphoglycerate into six molecules of glyceraldehyde 3-phosphate. The net product of the CBB cycle is one of the six molecules of glyceraldehyde 3-phosphate, with the other five molecules that are used in the regeneration phase of the cycle to produce 3 molecules of ribulose 1,5-bisphosphate that feed into the first reaction. The molecules of glyceraldehyde 3-phosphate that result from the CBB cycle can be used by the plant to produce starch or sucrose. Both Rubisco and other CBB enzymes are regulated in order to be active along with light-dependent photosynthesis. Rubisco, for example, has to be carbamylated to be active, a condition favoured by alkaline stromal pH and high stromal concentration of Mg^{2+}, which are indicators of active light harvesting and ATP synthesis ([16, 17]).

1.2 Energy dissipation and alternative electron flows

In plants, as mentioned in section 1.1, the main photosynthetic electron path spans linearly between PSII, PSI and is finalized with the reduction of $NADP^+$ to NADPH in a reaction mediated by FNR. Besides the linear electron flow, all photosynthetic organisms have developed several adaptations in order to dynamically tune light harvesting and electron flow in response to changes in metabolic and environmental conditions. Indeed, photosynthetic organisms exploit alternative electron flows to adjust the ATP/NADPH ratio and to respond to rapid variations in light intensity. In particular, sudden increases in light intensity can cause over-reduction of the photosynthetic electron transport chain, reducing the efficiency with which electron acceptors accept electrons from chlorophyll molecules within reaction centres.

When a reaction centre is reduced along with the downstream electron acceptors it is called a closed reaction centre, meaning that it can no longer drive photochemical reactions due to over-reduction. When excess light interacts with closed reaction centres without being dissipated it can lead to the formation of chlorophyll triplet states, which are stable enough to react with molecular oxygen and to consequently form singlet oxygen, which causes oxidative damage by reacting with biomolecules ([18]). Because of this, both photosystems display specific mechanisms to either dissipate excess energy, avoid over-reduction or efficiently repair damaged structures.

In particular, PSII is provided with an efficient mechanism of removal and substitution of damaged D1 core subunits – which are the ones meant to sustain most of the oxidative damage – called the PSII repair cycle ([19, 20]). Moreover, PSII is capable of dissipating excess energy as heat through the non-photochemical quenching (NPQ) of chlorophyll fluorescence. NPQ is induced rapidly during periods of light exposure as a result of the formation of the proton gradient across the thylakoid lumen, which is indeed exploited by the chloroplast as a sensor of photosynthetic activity and efficiency ([21]).

PSI, on the other hand, is protected from over-reduction and damage of the electron transport chain downstream of the RC (i.e. photoinhibition) by

mechanisms that divert electrons from Fdx-dependent enzymes to other acceptors. Such mechanisms are the cyclic electron flow (CEF) and pseudo-cyclic electron flow (pseudo-CEF).

1.3 Cyclic electron flow around PSI

The existence of a possible mechanism of cyclic electron flow around PSI was firstly proposed by Tagawa, K. *et al.* in 1963 as a light-dependent ATP phosphorylation mechanism in absence of production or consumption of reducing power ([22]). Indeed, through CEF, electrons are redirected from the acceptor side of PSI back to its donor side. This allows for the formation of the electrochemical proton gradient but prevents electrons from reaching FNR. Despite the proven importance of CEF in plant survival and growth, the role of the proposed CEF-mediating mechanisms remains unclear in many aspects, from their molecular effectors to their regulation. However, today it is accepted that CEF is mediated by two major known mechanisms that redirect electrons from the acceptor side of PSI to the PQ pool: the NDH-dependent route and the PGR5/PGRL1-dependent route (Fig 1.7). In land plants the NDH-1 complex is highly similar to the bacterial NADH-ubiquinone reductase (complex I of the respiratory chain) but it lacks the capability to bind NADH, and it has been proposed that it may exploit Fdx as an electron donor instead. However, it was demonstrated that the absence of NDH-1 in plants does not alter the q_E component of NPQ, which is pH-dependent, suggesting that NDH-mediated CEF does not heavily contribute to proton pumping across the thylakoid membrane. Moreover, NDH-1 is highly sub-stoichiometric in respect to PSI, suggesting the contribution of other pathways.

PGR5/PGRL1-dependent CEF was discovered through mutants in which the absence of either of these proteins causes the display of a low steady-state q_E. Although plenty of evidence demonstrates the involvement of PGR5/PGRL1 in CEF there is still no proof of their direct contribution in the redirection of electrons, which is in fact thought to be "unlikely" [22] due to PRG5 being a small soluble stromal protein, binding no cofactors, and whose absence does not alter CEF during induction of photosynthesis. PGRL1 is, instead, proved to be able to reduce quinones, but it is still sub-stoichiometric in respect to PSI and its absence does not translate in reduced maximal CEF rate [23].

Despite the uncertainty regarding the molecular mechanisms of cyclic electron transfer, numerous pieces of evidence classify CEF as a fundamental component of the photosynthetic electron transport as it appears to be involved in ATP synthesis, in the induction of NPQ and in the sensitivity to high-light and fluctuating-light stresses.

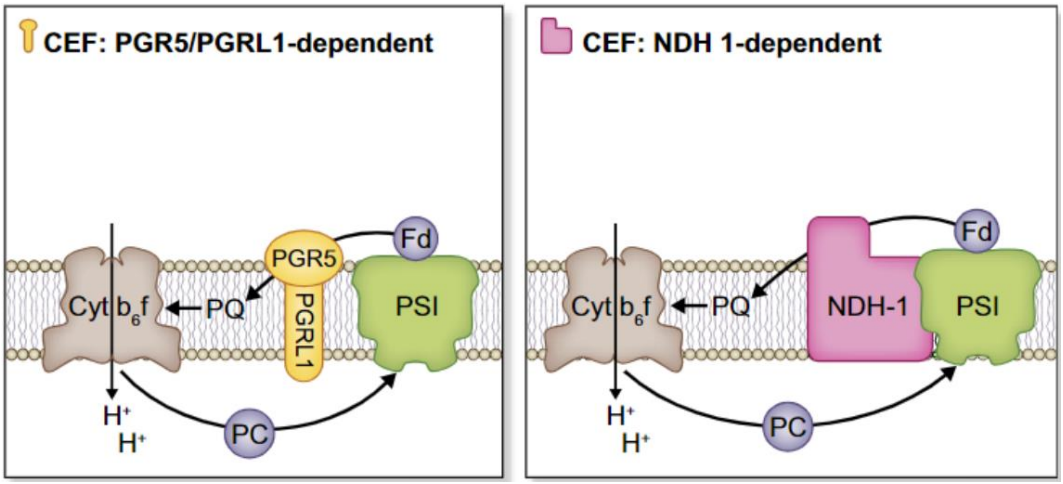

Fig. 1.7 – Figure depicting the two putative electron routes in CEF [24].

1.4 Pseudo-cyclic electron flow around PSI

Pseudo-cyclic electron flows, often referred to as water-water cycles, are mechanisms due to which electrons are redirected from the reduction of $NADP^+$ to the reduction of molecular oxygen to water (which is also the initial electron donor of the linear electron flow, hence the name water-water cycles). Such processes do not contribute to the production of NADPH, but they still allow formation of the proton gradient across the thylakoid membrane. Because of this, like CEF, also pseudo-CEF plays a role in the regulation of the ATP/NADPH ratio and in the photoprotection of PSI by acting as an additional electron sink that avoids over-reduction.

The main pseudo-CEF mechanisms consist of the Mehler reaction, initiated by the photoreduction of oxygen to hydrogen peroxide, and on the FLV-dependent reduction of oxygen. Photorespiration and the PTOX-dependent reduction of oxygen can also be considered water-water cycles, but they do not involve PSI directly [25]. The Mehler reaction is initiated by the direct photoreduction of oxygen to superoxide anion by electrons coming from the OEC in PSII:

$$2H_2O \rightarrow 4e^- + O_2 + 4H^+$$
$$2O_2 + 2e^- \rightarrow 2O_2^-$$

The superoxide anion is a highly reactive ROS, and it is rapidly disproportionated into hydrogen peroxide by the activity of the superoxide dismutase (SOD) located in the chloroplast. The hydrogen peroxide is rapidly scavenged by the ascorbate peroxidase (APX) before it can diffuse out from the chloroplast, producing monodehydroascorbate (MDA):

$$2O_2^- + 2H^+ \rightarrow O_2 + H_2O_2$$
$$H_2O_2 + 2\,ascorbate \rightarrow 2H_2O + 2\,MDA$$

MDA is an oxidized form of ascorbate, which is regenerated through reduction mediated by electrons coming from the LEF:

$$2e^- + 2H^+ + MDA \rightarrow ascorbate$$

The sum of all the aforementioned reactions is the simplified form of the Mehler reaction [26]:

$$2H_2O + O_2^* \rightarrow O_2 + 2H_2O^*$$

The Mehler reaction is thus a chloroplast-confined ROS detoxification mechanism which effectively subtracts electrons from photochemistry, with no net products, and hence it acts as an alternative electron sink in respect to Fdx-dependent enzymes and NADPH. Despite this, it has been demonstrated that the Mehler reaction is induced slowly and may not be able to respond to sudden changes in light intensity [27].
Pseudo-CEF can also be mediated by flavodiiron proteins (FLVs), which appear to be able to accept electrons downstream of PSI and to redirect them to the reduction of oxygen into water in a Mehler-like fashion. Pseudo-CEF, much like CEF, has been demonstrated to play a pivotal role in preventing photoinhibition of PSI through the phenotypic analysis of mutants, which show severe growth impairment when grown under fluctuating light. Indeed, while PSII is provided with efficient repair mechanisms which limit the severity of its damage, PSI photoinhibition has drastic effects on the capability of photosynthetic organisms to efficiently harvest light and, thus, to grow.

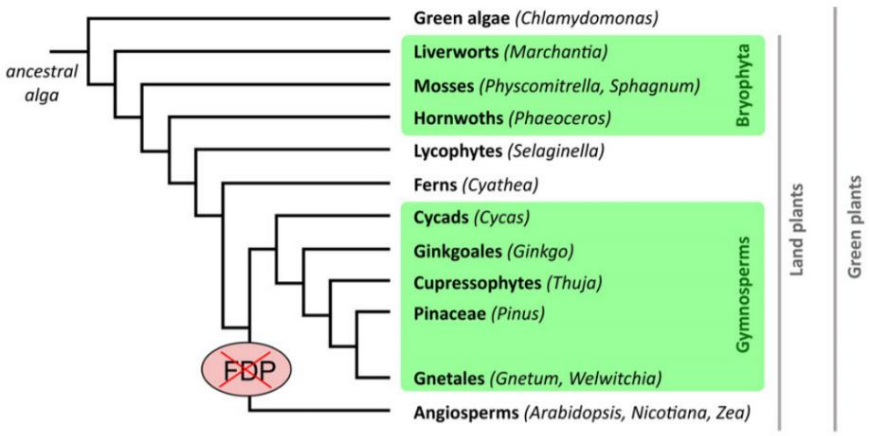

Fig. 1.8 – Phylogenetic tree of green plants. FLVs were lost during the evolution of angiosperms from the common ancestor with gymnosperms [27].

While the molecular effectors of the Mehler reaction (SOD and APX) are universally conserved across photosynthetic organisms, FLVs have been lost during the evolution of angiosperms, but they are present from cyanobacteria

up to gymnosperms (Fig. 1.8) [24, 25]. The fact that FLVs are present in most photosynthetic organisms raises questions regarding why they have been lost during the evolution of flowering plants and on what would be the consequence of their reintroduction.

1.5 Structure and function of flavodiiron proteins

Photosynthetic FLVs are part of the large family of flavodiiron proteins (FDPs), which are present from anaerobic prokaryotes up to higher photosynthetic eukaryotes. FDPs are enzymes provided with nitric oxide and/or oxygen reductase activity, and they are thought to have evolved as an adaptation mechanism for the removal of these potentially toxic compounds.

FDPs are soluble, modular metalloenzymes characterized by the presence of two core domains: a N-terminal metallo-β-lactamase-like domain provided with a diiron catalytic centre, where substrate reduction takes place, followed by an FMN-binding flavodoxin-like domain. FDPs typically receive electrons from rubredoxins or from NADH/FAD-dependent oxidoreductases [28]. Besides these two conserved domains FDPs of various organisms are characterized by the presence of additional domains, whose presence defines their class (Fig. 1.9).

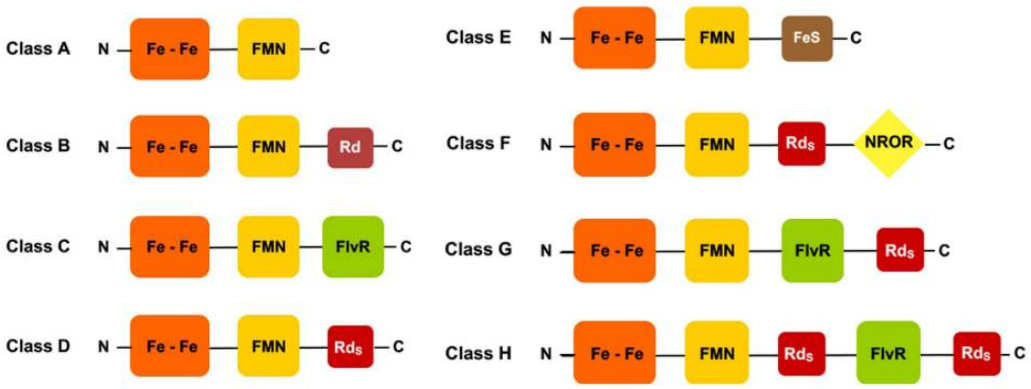

Fig. 1.9 – Modular representation of the eight known classes of FDPs [28]. (Fe-Fe: metallo-β-lactamase-like domain; FMN: flavodoxin-like domain; Rd: canonical rubredoxin domain; Rd_S: short rubredoxin domain; NROR: NADH:rubredoxin oxidoreductase domain; FlvR: flavin reductase-like domain).

While most FDPs belong to the class A, cyanobacterial FLVs are described as class C FDPs, being provided with a flavin reductase-like domain, and this class appears to be specific to oxygenic photosynthetic organisms [29]. The additional FlvR domain allows class C FDPs (FLVs) to putatively exploit NADPH as electron donor for the reduction of oxygen into water, although it is still uncertain which, between NADPH or reduced Fdx, is the actual electron donor [30].

While most FDPs are active as homodimers or homotetramers, the multimerization of photosynthetic FLVs is still to be clarified. In photosynthetic organisms FLVs are typically present in multiple homologous

genes, suggesting that they are active as heterocomplexes. This consideration is also supported by the fact that the knock-out of either *flva* or *flvb* genes in *Physcomitrium patens* affects the accumulation of both proteins [31]. The activity and organization of FlvA and FlvB proteins from *P. patens*, which are the ones expressed in the plants used in this work, was recently investigated by Beraldo, C. *et al.* (2024). The cited work provides evidence that these proteins do form heterocomplexes and that they are independently capable of performing a NADH/NADPH-dependent oxygen reduction.
The role of FLV-dependent pseudo-CEF in *P. patens* was determined through the analysis of mutants in which either FLVA or B was depleted [31]. Evidence demonstrates that FLVs are functional in the first instants after the onset of illumination with actinic light and that, when FLVs are absent, CEF mediates most of the electron transport in this period. Moreover, when FLV-depleted individuals are grown under fluctuating light they show a strong reduction in growth.

The impact of FLVs on photosynthesis in the organisms that naturally express them suggests that in angiosperms, which do not possess *flv* genes, FLV-dependent pseudo-CEF is completely substituted by CEF. When introduced in *Arabidopsis thaliana* and *Oryza sativa*, FLVs from *P. patens* enhanced the electron sink capacity and protected PSI from fluctuating light-induced over-reduction and PSI photoinhibition [32, 33]. This kind of evidence suggests that the introduction of a FLV-mediated alternative electron flow around PSI in angiosperms could provide an electron escape route for excess electrons, avoiding PSI over-reduction and consequent damage that results in photoinhibition and decreased yield.

2. Aim of the project

The role of FLVs in protecting the photosynthetic machinery from photodamage has been thoroughly investigated in *P. patens* as well as in cyanobacteria and in green algae, proving that these proteins serve as a "safety valve" that protects photosystem I (PSI) from excess electrons in the first seconds of light exposure [31]. Since FLV proteins are present in all photosynthetic organisms except for angiosperms, which include almost all the plants with agricultural importance, the aim of this project is to assess if the effects of FLV expression in such plants could result increased stress tolerance and productivity

The main aim of this project was to thoroughly investigate the effects of FLV accumulation on the photosynthesis of *Nicotiana tabacum* plants and to subsequently determine whether their presence results in increased resistance to fluctuating light conditions.

The secondary objective of this thesis was to generate and isolate transgenic *Solanum lycopersicum* plants expressing FLVs and to test their functionality.

The tertiary objective of this project was to obtain expression vectors for the expression of *flv* genes in *Hordeum vulgare*.

3. Materials and methods

3.1 Model organisms

All individuals were grown in a growth chamber, at 25°C and 45-65% of air humidity, following a photoperiod of 16h of light (100uE) and 8h of dark. This photoperiod was chosen as it is typical of a day during the growing season (i.e. the photoperiod of a summer day). Plants were transferred to the greenhouse facility for flowering and maintenance. *In vitro* cultures of *S. lycopersicum* were grown on ½ MS. Plants in pots were grown in universal soil added with 20% perlite.

3.1.1 *Nicotiana tabacum*

The species *Nicotiana tabacum*, Samsung variety, was the model organism of choice for the study of phenotypic manifestation of traits due to the presence of transgenic *flv* genes.

N. tabacum is a dicotyledonous, solanaceous species part of Angiospermae, and it is an annual herbaceous plant native to tropical and subtropical America. Its inflorescences are multi-branched panicles, with each flower being pinkish and hermaphrodite.

N. tabacum is widely used as a model organism in plant research due to its well-known genetics, its capability to produce large amounts of biomass and to its survivability *in vitro* and under greenhouse conditions, as well as the availability of a fully sequenced genome and its being prone to genetic transformation through *Agrobacterium*-mediated approaches.

N. tabacum T0, T1 and T2 seeds coming from plants transformed with both *flva* and *flvb* genes were already available in the laboratory. Only T2 individuals were used for phenotypic and physiological characterization. For genotyping, *N. tabacum* seeds were germinated in ½ MS (see Table 1) added with kanamycin (50mg/L). For other purposes, *N. tabacum* seeds were germinated on watered paper and, after full germination, were transferred in soil.

3.1.2 *Solanum lycopersicum*

The species *Solanum lycopersicum*, Florida Petite variety was used as a supplementary model organism for studying the effect of FLV protein expression *in vivo*, being it a species of commercial and nutritional interest.

S. lycopersicum is a dicotyledonous, solanaceous species part of Angiospermae, and it is a perennial herbaceous plant native to South America. It is mainly characterized by compound leaves and yellow, hermaphrodite flowers that upon fertilization give rise to soft berries.

S. lycopersicum is commonly used as a model organism for plants due to its being a plant of nutritional interest, as well as its well-characterized genetics and its capability to produce large amounts of biomass.

T2 seeds of one transgenic line of *S. lycopersicum* expressing FLVs were already present in the laboratory.

3.2. Plant transformation

3.2.1 *Solanum lycopersicum*

Before transformation, *S. lycopersicum* seeds must be sterilized. Approximately 100 seeds were placed in a 50mL falcon tube, where they were initially washed with 30mL of a solution containing 5% NaClO (sodium hypochlorite) and 0,1% Tween-20 for 20 minutes. After the initial wash, seeds were washed with 30mL of sterile H_2O for 5 minutes four additional times. Seeds were then sown in Magenta trays containing ½ MS medium (see table 1) in sterility, under biological hood, and were incubated at 4°C overnight for synchronization. Then, plates were transferred in the growth chamber (see conditions in section 3.1) for germination.

The transformation protocol from Fillatti *et al*. (1987) [34] was used for the generation of transgenic *S. lycopersicum* individuals. To initiate the transformation, previously sterilized seeds were sown in Magenta trays filled with ½ MS (see table 1). Along with the sowing, an *A. tumefaciens* LBA4404 starter culture was prepared by inoculating transformed bacteria in YEB added with streptomycin (100mg/L) and kanamycin (50mg/L) one week prior the transformation. The inoculum was refreshed three days prior to the transformation and incubated until the OD_{600} was around 1.2 and 1.5.

The day of the transformation, an aliquot of the *A. tumefaciens* inoculum was inoculated in liquid KCMS (see table 1) added with acetosyringone (0.2mg/L) to reach an OD_{600} of 0.1.

Fully grown cotyledons from 8-day-old wild-type Florida Petite individuals were detached from plantlets and cut at both ends. Sections were then transferred, with the lower page facing down, onto a solid KCMS plate added with acetosyringone to promote *A. tumefaciens* infection.

In these conditions the plates were then added with 15mL of the *A. tumefaciens* LBA4404 inoculum in liquid KCMS with OD_{600} equal to 0,1 mentioned before. Once the inoculum was added, plates were incubated for 15 minutes. Later, the bacterial suspension was removed, and cotyledons were incubated at 25°C for 48h in the dark.

After incubation, cotyledons were transferred in RGM1 medium (see table 1) added with antibiotics, with the lower page facing down and pressed against the medium. After 14 days cotyledons were transferred to RGM2 (see table 1), also provided with antibiotics, and such transfer was repeated once every two weeks until callus and shoot formation. Once shoots had formed and were developed enough, they had to be cut and placed in Magenta trays containing Rooting Medium (see table 1). Once rooted, plantlets were propagated and then transferred in soil. Plants were then grown in the growth chamber as previously mentioned.

Table 1

Solanum lycopersicum					
	½ MS	KCMS	RGM1	RGM2	RM
MS basal salt mixture	-	4.4g/L	4.4g/L	4.4g/L	-
Ms without vitamins	2.15g/L	-	-	-	2.2g/L
Morel vitamin mixture (1000X)	0.5g/L	-	-	-	-
Vitamin Nitsch (1000X)	-	-	1mL/L	1mL/L	1mL/L
1-naphtalenic acid	-	-	0.01mg/L	0.01mg/L	-
Riboside zeatin	-	-	2mg/L	2mg/L	-
Kinetin	-	0.1mg/L	-	-	-
Acetosyringone	-	40mg/L	-	-	-
2,4-D	-	0.2mg/L	-	-	-
Thiamine	-	0.9mg/L	-	-	-
Glycine	1mg/L	-	-	-	-
Myoinositol	0.05g/L	-	-	-	-
Glucose	500mg/L	-	-	-	-
Sucrose	10g/L	40g/L	30g/L	10g/L	10g/L
Potassium bisphosphate	-	200mg/L	-	-	-
Augmentin	-	-	1.08g/L	0.6g/L	0.3g/L
Kanamycin	-	-	100mg/L	100mg/L	75mg/L
Phytagel	-	-			3g/L
Agar	5g/L	6g/L	6g/L	6g/L	4g/L
pH	5.5	5.8	5.8	5.8	5.8

NB. Liquid KCMS is equal to solid KCMS except for the absence of 2,4-D.
NB. Antibiotics and phytohormones were added after autoclave.

3.3 Bacteria transformation

3.3.1 *Escherichia coli* transformation

DH5α thermo-competent *E. coli* is a widely used strain due to several useful characteristics, such as high insert stability due to *recA1* mutation, high yield and quality of purified DNA due to *endA* mutation and high transformation efficiency. DH5α cells were stored at -80°C. For the transformation, 100uL of DH5α suspension were slowly thawed in ice. Once thawed, a DNA aliquot was added to the suspension with a 1:10 volume ratio in respect to the suspension itself. The mixture was then incubated in ice for 20 minutes, during which the DNA accumulates around the surface of bacterial cells due to its negative charge. Then, the mixture was subjected to a heat shock at 42°C for 45 seconds. The heat shock is necessary to let the exogenous DNA be internalised by bacterial cells, as it induces the formation of pores and an overall increase in

membrane fluidity and permeability. The cells were then incubated 2 minutes in ice and then added with 500mL of LB (see table 2). After this step, the inoculum was incubated at 37°C for 45 minutes in agitation and then plated on Petri plates containing LB added with the antibiotic of choice (kanamycin or streptomycin and spectinomycin).
The plates were then incubated overnight at 37°C and later checked for bacterial growth, which is an indicator of the correct internalization of the exogenous DNA since it confers antibiotic resistance. Colonies were then tested for the presence of the correct sequence through colony PCR followed by DNA extraction and restriction analysis.

3.3.2 *Agrobacterium tumefaciens* transformation

Agrobacterium tumefaciens is a Gram-negative species part of the Rhizobiaceae family. It is widely used to generate transgenic plants due to its capability to penetrate damaged tissue and insert exogenous DNA within plant cells. In nature this bacterium is the etiologic agent of the crown gall disease, which consists in the formation of shooty tumours in plants caused by the insertion of the Ti plasmid. This plasmid bears the sequences required for the transfer and insertion in a host genome as well as the coding genes for the synthesis of auxins and cytokinins. This mechanism of infection can be exploited to insert wanted DNA sequences within plant genomes.
Indeed, the sequence of interest must be inserted within a plasmid provided with sequences recognized by Vir proteins, which are responsible for the mobilization and transposition of transposable regions.
The *A. tumefaciens* strain used in this work was LBA4404, which harbours streptomycin resistance and a Ti plasmid provided with *Vir* genes but incapable of self-transport.
For the transformation of *A. tumefaciens* LBA4404, 0.5-1μg of plasmid DNA were added to a 100uL bacterial suspension. The mixture was then sequentially incubated in ice for 5 minutes, in liquid nitrogen for 5 minutes and then at 37°C for 5 minutes more. After these steps, 1mL of YEB (see table 2) was added to the suspension, which was then incubated at 28°C for 4 hours. The resulting inoculum was then plated on solid YEB added with desired antibiotics (streptomycin and kanamycin) and incubated at 28°C for 3 days in the dark.
After three days, the plates were checked for bacterial growth and selected colonies were picked up and resuspended in 5mL of liquid YEB added with the same antibiotics as the step before. The inoculum was then incubated two additional days in the dark in agitation. At this point, the inoculum was tested through PCR for the presence of the desired DNA sequence. The inoculum was incubated until it reached an OD600 of at least 0.8. At this point the suspension can be diluted in the plant transformation medium and used for the transformation of plants (see section 3.2.1 for further details).

Table 2

	Escherichia coli	*Agrobacterium tumefaciens*
	LB	**YEB**
NaCl	10g/L	-
Yeast extract	5g/L	5g/L
Tryptone	10g/L	5g/L
Sucrose	-	5g/L
Beef sucrose	-	5g/L
$MgSO_4$	-	0.049g/L
Agar	15g/L	20g/L
pH	7	7

3.4 Molecular biology

3.4.1 Plasmid DNA purification from *Escherichia coli*

Purification of plasmid DNA from *E. coli* is a fundamental step in every cloning procedure since this species is commonly used to amplify wanted sequences. Plasmids within bacterial cells have been purified through the GeneJet Plasmid Miniprep Kit from Thermofisher.

Transformed DH5α cells were grown in either 5 or 10mL of liquid LB added with proper antibiotics at 37°C overnight. The suspension was then pelleted through a 5-minutes centrifugation at 12000 rpm. The bacterial pellet was then resuspended in the Resuspension Solution provided by the kit and then subjected to lysis thanks to the Lysis Solution, also provided by the kit. The alkaline pH of the resulting suspension was later neutralized with the Neutralization Solution, and the suspension itself was then centrifuged for 5 minutes at 12000 rpm for cellular debris and genomic DNA to sediment. The supernatant was then harvested and positioned within a GeneJet Column, which is provided with a membrane that selectively retains plasmid DNA.

The DNA was separated from the solution with a first 1-minute centrifugation at 12000 rpm and, after multiple washes performed with the Wash Solution provided by the manufacturer, the purified plasmid DNA was eluted from the column by using 70°C water.

The purified plasmid DNA was then quantified through either NanoDrop quantification or UV/VIS spectrophotometry. Good quality purifications tend to display an absorption peak at λ=260nm, with a 260/230 and 260/280 absorbance ratios both above 2. Quantification was always followed by restriction analysis.

3.4.2 DNA restriction

Restriction enzymes are bacterial endonucleases capable of performing double-strand DNA breaks with a sequence specificity determined by short palindromic sequences. Evolved as a sort of innate immunity towards exogenous DNA sequences, specific restriction enzymes show specific sequence preferentiality, and their activity on DNA molecules either generates

blunt or protruding DNA ends. Thanks to both these properties, restriction enzymes serve as a powerful tool to determine the identity of a DNA sequence and to allow the insertion of wanted sequences within specific regions.
DNA restriction with a restriction enzyme is specific only when performed at the correct temperature and in presence of the correct buffer, which are enzyme specific. DNA restriction has been performed, following the aforementioned requirements, both to insert a desired DNA sequence within vectors of interest in precise positions and to analyse results of ligations between inserts and destination vectors. The list of all the used restriction enzymes is in Table 3.

Table 3

Enzyme	Manufacturer	Buffer	Temperature [°C]
SfiI	NEB	RCutSmart	50
MluI	Thermo	R Buffer	37
XmaI	NEB	RCutSmart	37
SacI	Thermo	Tango Buffer	37

3.4.3 DNA dephosphorylation

Before ligation with the proper insert, the linearized destination vector must be dephosphorylated in order to prevent circularization, and this increases the efficiency of the ligation with the insert.
Dephosphorylation was performed with the Antarctic phosphatase from New England Biolabs (5000U/mL) in presence of the Antarctic phosphatase reaction buffer (10X) from the same manufacturer. One unit of Antarctic phosphatase is defined as the amount of enzyme required to dephosphorylate 1µg of a 3kbp vector cut with a restriction enzyme generating 5' recessed ends in 30 minutes at 37°C. 1µg of a 3kbp vector cut as aforementioned generates 1pmol of DNA ends, and all dephosphorylation reactions were scaled to respect this proportion.

3.4.4 DNA ligation

The ligation reaction consists of the formation of a phosphodiester bond between a 3'-OH and a 5'-PO_4 nucleic acid terminus. Ligation between insert and destination vector was performed using the T4 DNA ligase from New England Biolabs (400000U/mL) in presence of the T4 DNA ligase reaction buffer (10X) from the same manufacturer. One unit of T4 DNA ligase is defined as the amount of enzyme required to ligate 50% of HindIII fragments of λ DNA in a total reaction volume of 20µL at 16°C.
All ligation reactions were properly scaled following the definition and performed in a volume of 20µL with different proportions of linearized dephosphorylated destination vector and insert, from 1:3 up to 1:7.

3.4.5 Polymerase Chain Reaction and applications

The Polymerase Chain Reaction is a standard molecular biology technique that exploits thermo-resistant DNA polymerases and sequence-specific primers in order to amplify desired sequences starting from low quantities of a DNA template. All primers used in this thesis are listed in Table 4.

All PCR reactions follow three main steps that are iterated a variable number of times.

1. The first step is the denaturation of the double-stranded DNA template, performed at 96°C for 30 second, which is required to expose the sequence to which the primers have to anneal. In specific applications, such as in Colony PCRs, this step may be preceded by a longer period at 96°C that causes bacterial membranes to degrade.
2. The second step is the annealing of primers to the template, performed for 30 seconds at specific temperatures typically between 55°C and 65°C depending on the sequence of the primer couple used. Specifically, the annealing temperature in this step is determined by the melting temperature (Tm) of the primers, which is itself determined by their GC content. The annealing temperature used in PCR is typically equal to the lowest melting temperature between the two primers.
3. The third step is the extension of the amplicon, performed at 72°C and for a duration that varies depending on the length of the amplicon and on the processivity of the DNA polymerase in use. In this step the polymerase extends the amplicon starting from the primers by catalysing the formation of phosphodiester bonds between dNTPs complementary to the sequence of the template to amplify. This step generates a collection of double-stranded DNA molecules, doubling the starting concentration of the template.

These three steps are repeated up to 40 times within a thermocycler in order to exponentially amplify the sequence delimited by the forward and reverse primer couple. Once the iterations have been completed one final extension is performed at 72°C for 5 minutes in order to fully elongate all potential protruding ends of the amplicons.

All PCR reactions in this thesis have been performed using ThermoScientific DreamTaq DNA polymerase, and all PCR products have been checked through gel electrophoresis.

Table 4.

Primer name	5'-3' Sequence
35S Forward	GGGGAATTCGGTGGCTCCTACAAATG
FlvA seq 3	AACAGGCAGTGGGTAGAGTG
FlvA seq rev 1	CACCCTAACATCTGCCTCCT
FlvB seq rev 1	CACTCTGAGTCTGAATGCGC
EF1α Forward	TGAGAAAGAAGCTGCTGAGATG
EF1α Reverse	AGAAACCTCCTTCACGATTTCA

3.4.6 Agarose gel electrophoresis

Agarose gel electrophoresis is a standard molecular biology technique which employs gels made with variable quantities of agarose to separate DNA molecules based on their molecular weight, which is proportional to the length of their nucleotide sequence. In particular, agarose gel electrophoresis exploits the supercoiled helical agarose matrix within the gel, which is made of pores and channels that allow DNA molecules to move without diffusing.

The intricate molecular structure of an agarose gel opposes the migration of negatively charged DNA molecules when an external electric field (E) is applied, making the amount of their displacement inversely proportional to their dimensions. DNA molecules are negatively charged, with a net charge proportional to the amount of phosphate groups the molecule bears, which is one per base. Thus, the net negative charge of DNA molecules increases with their molecular weight, but their charge-to-mass ratio is uniform. Because of their charge, when an external electric field is applied, DNA molecules migrate towards the anode (positive electrode). The electrophoretic mobility of a DNA molecule is inversely proportional to the frictional force DNA molecules are subjected to, which is defined by pore dimension, viscosity and by the dimension of the molecules.

By this definition, the mobility of a DNA molecule in an agarose gel is mostly influenced by its dimension, which is a function of its molecular weight, and by the dimension of the pores, which is determined by the concentration of agarose.

To perform gel electrophoresis, 1.2% and 1% agarose gel were prepared by dissolving 1.2g or 1g of gel-grade agarose every 100mL of TAE 1X (40mM Tris-acetate, 1mM EDTA), respectively. Because of the relatively low solubility of agarose polymers, when placed in water the resulting mixture was heated until boiling. Once clear, SERVA DNA Stain G was added to the solution with a 1:200000 dilution for DNA molecules to become visible once illuminated with UV light. The staining consists of an intercalating agent that emits green fluorescence upon UV illumination when bound to nucleic acids.

The completed solution is then poured into moulds provided with a comb with the desired number of wells for sample loading. Before loading, samples were prepared through addition of TriTrack DNA Loading Dye by ThermoFisher Scientific, with a 1:6 dilution. The loading dye limits the diffusion of DNA molecules and allows for the visualization of the migration front. Once the gel was solidified, samples were loaded along with the GeneRuler molecular weight marker by ThermoFisher Scientific, which is needed to determine the exact dimensions of the separated DNA fragments. DNA migration was assessed after 30 minutes of running at 110mV, and gels were analysed through UV exposure through a transilluminator or by using a GelDoc XR platform by BioRad.

3.4.7 Immunoblot

Immunoblotting is part of electrophoresis-based molecular biology approaches through which it is possible to separate the proteins contained in heterogeneous samples and to selectively assess presence and quantity of specific targets through the use of antibodies.
The first step of immunoblotting is, indeed, the electrophoretic separation of proteins. There are several types of protein electrophoresis techniques that separate proteins based on different properties, such as SDS-PAGE, BN-PAGE, isoelectric focusing and 2D-PAGE. In this work only SDS-PAGE was used, which exploits the denaturing and charge-uniformizing properties of sodium dodecyl sulphate (SDS) to separate proteins only based on their molecular weight.
In Western Blotting, after electrophoretic separation the proteins are transferred to a polyvinyl fluoride (PVDF) or nitrocellulose membrane through blotting, and the membrane is then incubated with protein-specific primary antibodies and secondary antibodies for protein visualization and quantification. In this work, SDS-PAGE was followed by transfer to nitrocellulose membranes, and proteins were visualized through nitro blue tetrazolium (NBT) – 5-bromo-4-chloro-3-indolyl phosphate (BCIP) assays.

Gels for protein electrophoresis were prepared using polyacrylamide, which is an acrylamide polymer that forms, after the casting of the gel, through a polymerization reaction between acrylamide, ammonium persulfate and TEMED. The polymerization and cross-linking reactions form a three-dimensional matrix that opposes the migration of proteins. Besides polyacrylamide, another fundamental component of the gel is SDS, which is an anionic detergent that denatures the proteins within the samples and uniforms their net charge to -1. The presence of SDS excludes the contribution of charge differences to the electrophoretic mobility of the proteins and determines the direction of their migration from the negative electrode, the cathode, to the positive electrode, the anode. Thus, SDS allows for the separation of denatured proteins only on the basis of their molecular weight.
Gels for protein electrophoresis were prepared so that the composition of the upper portion is different from that of the lower part.
Specifically, the upper portion of a gel for protein electrophoresis is called the stacking gel; it was prepared with lower acrylamide concentration (4%), and it has lower pH (6.8). When within the stacking gel, the proteins are stacked by the presence of hydrochloric acid in the gel medium and of glycine in the running buffer. At pH 6.8 glycine is mostly in its zwitterionic form, hence it has lower electrophoretic mobility than the proteins, and it forms a “trailing edge”, while chloride ions have a much higher electrophoretic mobility and form a “leading edge”. Because of this, sample proteins are concentrated within narrow bands, ensuring that they all reach the running gel at the same time. The concentration of the different components for both the stacking and the running gel are listed in Table 5. Once prepared, the running and the stacking

gels are poured sequentially between two glasses and a comb is added to form the wells.

Sample preparation is a key step in SDS-PAGE as well as in all the immunoblotting procedures. In this work, leaf disks obtained by mature leaves of living WT and FLV plants were used for protein extraction. Leaf disks were detached from leaves, inserted in 1,5mL Eppendorf tubes and rapidly submerged in liquid nitrogen, and were later conserved at -80°C.
On the day of SDS-PAGE, samples were removed from -80°C storage and submerged in liquid nitrogen once again. While frozen, leaf disks within the tubes were homogenized by pestellation. Once completely disintegrated, 100µL of SB 3X (see Table 6) with DTT were added to the sample. The Sample Buffer contains both SDS, which denatures the proteins and confers a homogeneous negative charge, and DTT, which is a reducing agent that reduces cysteines in order to break disulphide bonds. Samples were then centrifuged at 13000 rpm for 10 minutes at room temperature in order for cellular debris to separate. The resulting solution was dark green, and a correct extraction forms a white pellet at the bottom of the tube. Whenever the pellet was still green, additional 50µL of SB 3X + DTT were added, and the procedure was repeated. The supernatant was then transferred to new Eppendorf tubes while being kept cooled and in the dark. Then, for each sample, 5µL of supernatant were transferred to a new tube and 170µL of acetone were added in order to obtain a ratio of 1:35. The solution was centrifuged at 13000 rpm for 5 minutes to precipitate the proteins, and the resulting supernatant was used for the quantification of chlorophylls. 80µL of the acetonic extract of each sample were transferred to a cuvette and the absorbance of the sample between 600 and 750nm was scanned with a Cary 60 UV-Vis spectrophotometer by Agilent Technologies. The quantification was performed one or two times per sample, and chlorophylls were quantified by using the following equation:

$$Chl\ \left[\frac{\mu g}{mL}\right] = 35[20.20(OD_{645} - OD_{750}) + 8.02(OD_{663}\ -\ OD_{750})]$$

Chlorophyll quantification is performed to determine the amount of material required by each sample to load the same quantity of proteins in each well. Once the sample that requires the highest volume in order to load the desired amount of chlorophyll was identified, all of the aliquots from the other samples were isolated and added with the appropriate amount of SB 1X to reach equal volumes. Once correctly aliquoted, samples were denatured at 100°C. The gel, along with its glass support, was mounted in a Mini Trans-Blot cell (BioRad) filled with Running Buffer (see Table 7), and denatured samples were loaded along with a molecular weight marker.

Protein gel electrophoresis was performed through the application of a current supplied by the PowerPac Universal Power Supply by BioRad. Current was applied at 30V for 30 minutes, followed by 110V supplied until complete removal of chlorophylls.
Once the electrophoresis was completed, the gel was removed from the support and submerged in Transfer Buffer (see Table 7). While submerged, the gel was placed in direct contact with a nitrocellulose membrane. Both were then placed in contact, at both sides, with thick filter paper foils and with two sponges. The so-called "sandwich" was mounted in a support for the transfer procedure to occur. Transfer was performed in the same Mini Trans-Blot cell as the running step, filled with Transfer Buffer, at 100V for 1 hour or overnight at 30V and 4°C. Once completed, the success of the procedure was tested by staining the membrane with Ponceau red, which is a removable red staining that allows for the direct visualization of the transferred proteins in each lane.

Correctly prepared membranes were then incubated with TBS + 10% milk (see Table 8) for 1 hour at room temperature or overnight at 4°C to "block" the membrane to avoid non-specific binding of the primary antibody to off-target proteins. Once blocked, the membrane was washed six times, for ten minutes each, with TBS to remove excess milk and residual Ponceau traces. After that, the membranes were incubated 2 hours with aliquots of different primary antibodies (see Table 9) and were then washed six additional times with TTBS (see Table 8) as before. The primary antibodies used in this work were either commercially available (from Agrisera), custom-made or in-house made. Each primary antibody is prepared by immunizing a host of choice with an exposed epitope of the protein of interest. The host will naturally produce antibodies specifically directed against the injected epitope, which can then be purified and used for scientific applications. After the six TTBS washes, the membranes were incubated for 1 hour with a 1:10000 diluted aliquot of secondary antibody. The secondary antibody is directed against the constant region of the primary antibody, and it is also conjugated with an enzyme. The secondary antibodies used in this work were conjugated with alkaline phosphatase which, in the presence of BCIP and NBT, catalyses a reaction that forms an intense insoluble purple precipitate that can be used for visualizing proteins and for their colorimetric quantification using a ChemDoc platform.

Table 5.

	Stacking gel (4%)	Running gel (12%)
Tris-HCl pH 8.3 3M	-	1.24mL
Tris-HCl pH 6.8 0.313M	125µL	-
Acrylamide 40%	333µL	3mL
APS 10%	35µL	30µL
TEMED	24µL	20µL
SDS 10%	60µL	100µL
H_2O	3.43mL	5.66mL

NB. This table lists the components for one 1,5mm thick acrylamide gel.

Table 6.

	Sample Buffer 3X
Tris-HCl	125mM
Glycerol	30%
SDS	9%
DTT	100mM

Table 7.

	Running Buffer 10X	Transfer Buffer 10X
Tris pH 8.3	250mM	20mM
Glycine	1.92M	152mM
SDS	1%	-
Methanol	-	20%

Table 8.

	TBS 20X	TTBS 1X
Tris-HCl pH 7.4	0.4M	0.02M
NaCl	3M	0.15M
Tween-20 20%	-	1%

Table 9.

	Dilution
α - FlvB	1:500
α - PsbD	1:1000
α - LhcII	1:1000
α - PsbS	1:2000
α - PsaA	1:2000
α – PsaD	1:1000
α – RbcsL	1:100000
α – γATPase	1:1000
α -Cyt *f*	1:1000
α - NdhH	1:10000

3.5 Vectors and cloning strategies

3.5.1 *Nicotiana tabacum* and *Solanum lycopersicum*

The vector used for the expression of FlvA and FlvB proteins in both *Nicotiana tabacum* and *Solanum lycopersicum* was prepared previously by Dr. Andrea Sabia under the supervision of Prof. Alessandro Alboresi.
The construct carrying *flv* genes was designed and used by Yamamoto, H. *et al.* (2016) [30] and it consists of both *flvA* and *flvB* genes from *Physcomitrium patens* spaced by a sequence encoding for the self-cleaving 2A peptide of the foot-and-mouth disease virus. In this way a 1:1 expression stoichiometry is

achieved for both genes. The construct is positioned under the control of the 35S promoter of the mosaic virus, which is strong and constitutive (Fig. 3.1a). The whole 35S::FlvA-2A-FlvB construct is also flanked by *attL* sites, which are the recognition sites for an LR clonase. The construct was inserted into an entry vector through a BP clonase, and the entry vector was then amplified through bacterial transformation. The entry vector was purified, and the construct was then cloned into the final vector (pBinAR) directly from the entry clone through an LR clonase (Fig. 3.1b) This cloning strategy is referred to as Gateway Cloning.

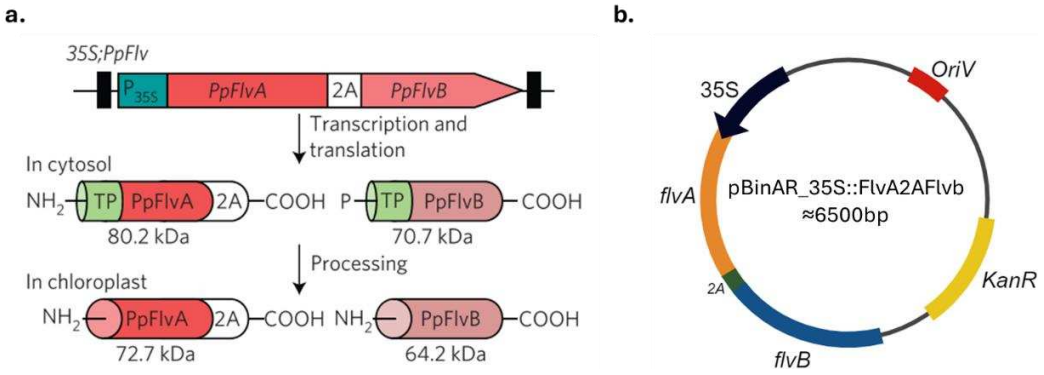

Fig. 3.1 – a) Schematic representation of the Flv-carrying construct from Yamamoto, H. *et al.* and its post-translational processing towards the chloroplast (TP: transit peptide) [31]. b) Schematic non-in-scale representation of the final expression vector carrying the construct of interest.

The final expression vector pBinAR_35S::FlvA2AFlvB carries a gene ensuring kanamycin resistance for screening and the OriV replication origin along with the construct of interest. The plasmid was verified through PCR and transformed into *A. tumefaciens* LBA4404 in order to perform Agrobacterium-mediated transformation of both *N. tabacum* and *S. lycopersicum*.

3.5.2 *Hordeum vulgare*

The successful expression of FlvA and FlvB proteins in *H. vulgare* could not rely on the construct by Yamamoto, H. *et al.* since the 2A peptide is not optimized to efficiently function in barley. To overcome this problem, *flvA* and *flvB* genes of the said construct were independently amplified using primers provided with additional endonuclease recognition sites. This procedure was performed by Dr. Andrea Sabia. As part of this project, the resulting PCR products were purified using a PCR Purification Kit by ThermoFisher Scientific and were subjected to the activity of the desired restriction enzymes (XmaI and MluI). The products were then cloned into the sub-cloning vector CPGE_VEC00103. This step was necessary in order to put both genes under the control of a ubiquitin (Ubi1) strong promoter from maize. Once the correct cloning of both genes into their respective sub-cloning vectors was verified, the aim of this work shifted to the cloning of the Ubi1::FlvA and the Ubi1::FlvB

constructs into their final expression vectors, CPGE_VEC00113 (see section 4.1).

3.6 Dual-PAM 100

The Dual-PAM 100 (Pulse Amplitude Modulation) is a P700 and chlorophyll fluorescence measuring system from Heinz Walz GmbH. It consists of a chlorophyll fluorometer, able to analyse PSII efficiency and activity, and of a dual wavelength absorbance spectrometer to analyse PSI.

PSII activity can be analysed by PAM instruments through the Saturating Pulse (SP) method thanks to the assumption that P680* excitation energy has only four possible and competing fates: photochemistry, non-photochemical energy quenching (NPQ), fluorescence and energy decay. When a SP is supplied to a photosynthetic sample it saturates the photosynthetic electron transport chain downstream of the reaction centres (i.e. it closes the RCs), excluding photochemistry from PSII energy conversion and allowing for the measurement of chlorophyll fluorescence in absence of photochemistry.
When a SP is supplied to dark-adapted samples, in which all reaction centres are open, the resulting block of photochemical reactions permits the measurement of the maximal chlorophyll fluorescence, F_m. When compared to the basal fluorescence induced by the presence of a measuring light, F_0, the ratio of the difference between F_m and F_0 and F_m itself provides indication of the theoretical maximal PSII quantum yield:

$$Max\ PSII\ efficiency = \frac{F_m - F_0}{Fm} = \frac{F_V}{F_m}$$

The same measurements, carried out in presence of actinic light (AL), allow for the determination of chlorophyll fluorescence under steady state actinic illumination, F, and upon the supply of a SP, F_m'. These parameters can not only provide information regarding the effective quantum yield of PSII Y(II) but, through the equations derived from Klughammer & Schreiber (2008) [35], they can also provide information about NPQ and non-regulated energy dissipation (NO). The sum of the effective quantum yield of PSII and of the yields of both NPQ and NO is equal to 1, which represent 100% of the energy conversion in PSII:

$$Y(II) + Y(NPQ) + Y(NO) = 1$$

Energy conversion at PSI happens when the electromagnetic energy, harvested by antenna complexes, is funnelled towards the P700 reaction centre. The excitation energy of P700*, like P680*, has different possible fates: photochemistry, fluorescence or dissipation as heat. However, unlike PSII, the fluorescence yield of PSI is independent of the redox state of the reaction

centre and cannot be exploited to probe its activity. Moreover, there is no evidence of regulated energy dissipation in PSI.
Because of these two properties, the photochemical quantum yield of PSI is only defined by the redox state of the reaction centre and of its acceptors: it is maximal (=1) when P700 is reduced *and* the acceptors are oxidized, and it is minimal (=0) when P700 is oxidized *or* when the acceptors are reduced. Consequently, complete energy conversion in PSI can represented as a sum of the photochemical quantum yield Y(I) and of the quantum yields of non-photochemical energy dissipation due to donor- *or* acceptor-side limitations Y(ND) and Y(NA), respectively [36]:

$$Y(I) + Y(ND) + Y(NA) = 1$$

Each PSI reaction centre can be found in three different states, and therefore all the PSI RCs are part of three different fractions (a, b, c) representing the said states, the sum of which is the totality of P700 RCs:

Fraction a: P700 is oxidized, and the acceptors are reduced: the reaction centre is closed. $Y(I) = 0$; $Y(ND) = 1$; $Y(NA) = 0$

Fraction b: P700 is reduced, and the acceptors are oxidized: the reaction centre is open. $Y(I) = 1$; $Y(ND) = 0$; $Y(NA) = 0$

Fraction c: P700 is reduced along with the acceptors: the reaction centre is closed. $Y(I) = 0$; $Y(ND) = 0$; $Y(NA) = 1$

When the fractions a, b and c are known, and knowing that the sum of all of them corresponds to the totality of PSI RCs in the sample, each quantum yield can be easily calculated:

$$Y(I) = b/a + b + c$$
$$Y(ND) = a/a + b + c$$
$$Y(NA) = c/a + b + c$$

The redox state of P700 reaction centres can be probed via measurement of the difference in absorbance between 875nm and 830nm. This difference is indeed minimal when P700 is completely reduced, in dark-adapted samples, and increases upon oxidation. Complete oxidation of P700 can be induced through the supply of a SP in presence of far-red light, and this procedure allows for the determination of P_m.
The P_m parameter represents the signal associated with complete P700 oxidation and is thus proportional to the totality of all P700 RCs (a + b + c). Complete P700 reduction is instead achieved through cessation of far-red illumination, and the signal measured in this condition is called P_0.
In the presence of actinic light, a donor-side limited fraction of P700 RCs is stably closed and oxidized; the signal measured in this condition is called P and it is proportional to the fraction (a).
When a SP is supplied in presence of actinic light illumination, all the open P700 RCs are oxidized, corresponding to the P_m' signal: the difference between P_m' and P signals is proportional to the fraction (b). The fraction (c) of

acceptor-side limited P700 RCs, which cannot be oxidized, is instead proportional to the difference between P_m and P_m' (Fig. 3.2).

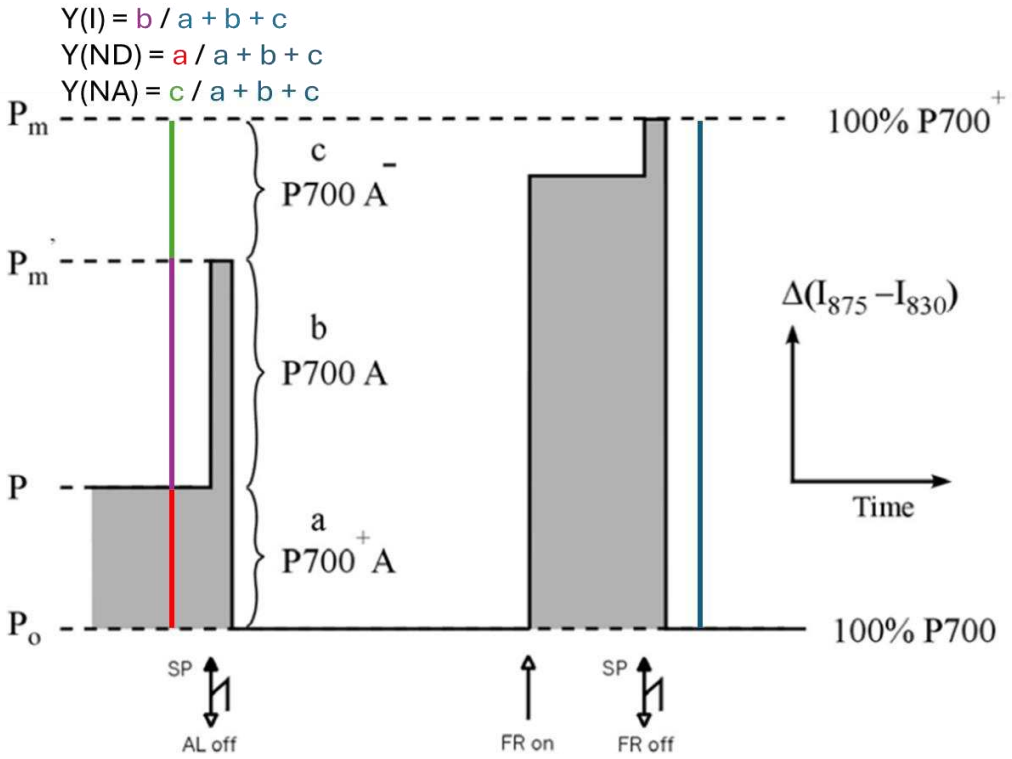

Fig. 3.2 – Principles of the Saturation Pulse method applied for the analysis of energy conversion in PSI. Adapted from Klughammer, C. & Schreiber, U. (2008) [36]. (SP: saturation pulse; AL: actinic light; FR: far-red light).

The plants used for Dual-PAM 100 measurements were dark-adapted 40 minutes before each experiment. Each experiment was carried out on plants grown in the same conditions (see section 3.1), of the same age and on mature leaves of similar leaf nodes when possible.

3.6.1 Dark-to-light P700 redox kinetic

Previous work (e.g. Ilìk, P. *et al.,* 2017) [25] has demonstrated that, when FLVs are present and functional, the redox kinetic of P700 upon dark-to-light transitions is characterized by a fast oxidation followed by an equally fast reduction, to which follows a slower re-oxidation that is not measurable when FLVs are absent (see Supplementary Materials, Fig. S5). Such trend is due to FLVs acting as an efficient electron sink downstream of PSI that keep it in an oxidized state during low-to-high light transitions. This can be measured through the dark-to-light fast light protocol, that consists of supplying six seconds of high actinic light (2000µE) followed by darkness to dark-adapted samples. This protocol was used to rapidly screen transgenic plants for the presence of functional FLVs. Since this protocol was used to screen young plantlets, the measurements were rapidly carried out on detached leaves that were big enough to cover both the lamp and detector of the instrument.

3.6.2 Fluctuating light protocol

The fluctuating light protocol is a standard protocol that is widely used to reliably quantify both PSII and PSI photosynthetic parameters. This protocol consists of subjecting dark-adapted plants to three cyclic low-to-high light transitions. Specifically, dark-adapted plants were exposed to 5 minutes of low light (63μE) followed by one minute of high light (1619μE) for three times.

3.6.3 Repeated Saturating Pulse protocol

The repeated Saturating Pulse protocol (rSP) is a relatively fast light protocol in which the leaves of dark-adapted plants are subjected to a first SP, used for P_m determination, followed by a series of six, one-second-long saturating pulses supplied with 10 seconds intervals between each other.
This protocol can be applied with no background actinic light as well as with high background light, and it allows for the quantification of the percentage of oxidized P700 RCs in respect to the total number of P700 RCs. In this work the rSP (2000μE) protocol was applied with a low actinic light background (70μE) for the quantification of oxidized P700 in light conditions that were similar to growth conditions.

3.7 JTS-10

The JTS-10 (Joliot-Type Spectrophotometer) is a LED pump-probe spectrophotometer designed for the measurement of electron transfer processes in photosynthetic organisms through fluorescence and absorbance changes. Pump-probe spectroscopy allows for the study of electron dynamics by exploiting light pulses that are split into two beams: a stronger one (the pump) which illuminates the sample and a weaker one (the probe) which is used as a reference to monitor the pump-induced changes in the optic properties of the sample itself.
As mentioned in the introduction, one of the results of photosynthetic activity is the generation of an electrochemical proton gradient ($\Delta\mu_{H^+}$) across the thylakoid membrane, which is described by an electric potential component ($\Delta\psi$) and by a gradient of proton concentration component (ΔpH).
The transmembrane electric field, generated by the electric potential gradient, induces absorbance peak shifts of pigments within antenna complexes due to a phenomenon known as electrochromic shift (ECS, Fig. 3.3a). The ECS, being a function of the electric field generated by the existence of a $\Delta\psi$, can be exploited as a membrane voltmeter and ammeter. One of the main problems with the exploitation of the ECS signal is that its measurement, usually carried out at λ=520nm, shows significant spectral overlap with other, field-independent phenomena. On timescales that range from seconds to minutes the generation of the ΔpH across the thylakoid membrane causes structural rearrangements that lead to scattering. Specifically, the scattering-induced

artifacts at 520nm can be accounted for by subtracting the ECS signal measured at 546nm.

Measurements of the ECS upon laser flashes (Xenon protocol) allows for the identification of a phased ECS response: less than 100μs after the flash a rapid increase in ECS signal is measured as a result of Δψ generation due to charge separation at the photosystems. This initial phase is followed by a slower rising of the ECS signal due to Cyt *b*6f activity, and after the cessation of illumination a decay of the ECS signal is measured due to the activity of the chloroplast ATPase and to ion leakage. The application of the Xenon protocol and the measurement of the amplitude of the first phase gives an indication of the number of active photosystems, and the use of inhibitors like 3-(3,4-dichlorophenyl)-1, 1 dimethylurea (DCMU, a well-known PSII inhibitor) can provide information regarding the PSII/PSI stoichiometry (Fig. 3.3b) [37].
Measurements of the ECS under continuous illumination require the distinction of the ECS signal from other, field-independent optical changes like the formation and decay of carotenoid triplet states. The DIRK protocol (Dark Interval Relaxation Kinetics; Sacksteder, C. *et al.* 2000) allows for ECS measurements both when steady-state photosynthesis is driven by continuous illumination and when the light is briefly switched off. The rate of membrane potential formation (V_{ph}), proportional to the electron transport rate, can be broken down into its molecular components. According to Bailleul, B. *et al.* (2010):

$$ECS \propto V_{ph} = R_{ph} + R_{b6f} - R_{leak}$$

Where R_{ph} is the photochemical rate of membrane potential formation, R_{b6f} is the Cyt b_6f specific rate and R_{leak} is the rate of ion leaking through the membrane. During continuous illumination, all these contributions are characterized by a specific value but, when the actinic light is switched off during the DIRK protocol, R_{ph} rapidly drops to 0. R_{ph}, which represents the photochemical electron transport rate, can therefore be calculated as the difference between the slopes of the ECS signal measured immediately before and after the light is switched off (Fig. 3.3c).

3.7.1 ETR measurements and DCMU treatment

In this work the JTS-10 was used to measure the ETR of 2.5 months-old, dark-adapted *N. tabacum* plants through the DIRK protocol applied at 520 and 546nm for scattering correction. ECS values were normalized using plant-specific PSI+PSII measured through the Xenon protocol. Measurements were carried out on attached leaves.
The JTS-10 was also used for the same type of measurements carried out in presence of DCMU. Two 1cm^2 dark-adapted leaf samples were detached from each 3 months-old WT and FLV plant used in the experiment. For each plant,

one of the two leaf samples was positioned between two paper sheets soaked with water to serve as a control, while the other was positioned between two paper sheets soaked with an 80µM DCMU solution. ECS measurements were carried out after a 1h-long treatment for both the control and the DCMU-treated samples.

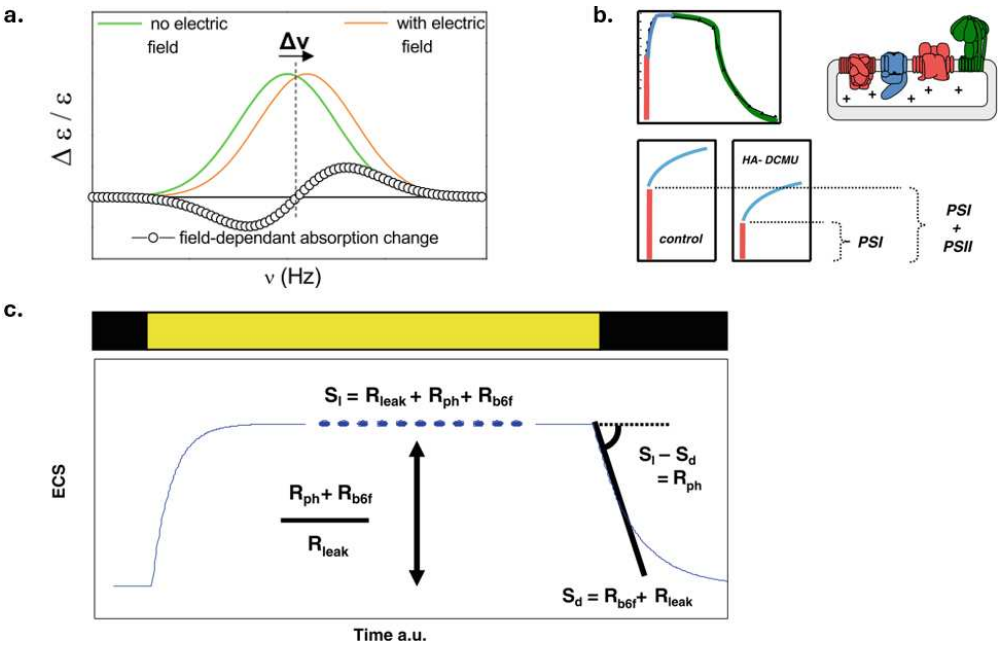

Fig. 3.3 – a) Representation of the field-induced absorbance peak shift that causes the appearance of a double-wave shape indicating the field-dependent absorption change. b) Schematic representation of the response of the ECS signal upon illumination with a saturating pulse. Each colour represents a phase of the ECS response due to a different molecular mechanism. c) Representation of the rationale behind the DIRK protocol. At the steady state of photosynthesis, the ECS signal is the result of the contribution of R_{ph}, R_{b6f} and R_{leak}, but when the light is switched off the R_{ph} contribution drops to 0 and the difference in the ECS slope between the two phases allows its determination. Adapted from Bailleul, B. *et al.* (2010) [37].

3.8 Fluctuating light growth stress

3 weeks-old *N. tabacum* plants were subjected to growth stress under fluctuating light. WT and FLV plants were germinated on watered paper (as specified in section 3.1.1) and were transferred in soil once completely germinated, approximately one week after sowing. Plantlets were initially positioned in germinators and, one week later, were transferred in single pots (Ø = 9cm) where both control and treated plants stayed for the duration of the experiment. Control plants were grown in growth chamber conditions (see section 3.1). Treated plants were positioned under a Photon System Instruments LED light (model SL 3500) and subjected to 4.5 minutes at 50µE followed by 30 seconds at 1000µE. The photoperiod for both treated and control plants was 16 hours of light and 8 hours of darkness, which is the

photoperiod of a typical day during growing season. Treated plants were grown in growth chamber at 16°C as an additional stress, as it slows down biochemical reactions such as those of the CBB cycle.
Since the space under the lamp was limited to 8-10 pots, the experiment was repeated three independent times. The Fv/Fm ratio of WT and FLV plants, both treated and control, was measured daily through an IMAGING-PAM instrument by Heinz Walz GmbH. Pictures of each plant were taken once every three days for canopy surface estimation through ImageJ (Fig. 3.4). The P_m of treated and control plants of the third batch was also measured through the use of the Dual-PAM. Each fluctuating light growth stress experiment lasted 14 days, and after every experiment the aerial part of each plant was collected for the measurement of the fresh weight. The aerial part of each plant was then dried at 60°C for 72 hours for the measurement of the dry weight.
Plants were dark-adapted for 40 minutes before the measurement of every photosynthetic parameter, and measurements were always performed between 9.30-11.30 a.m.

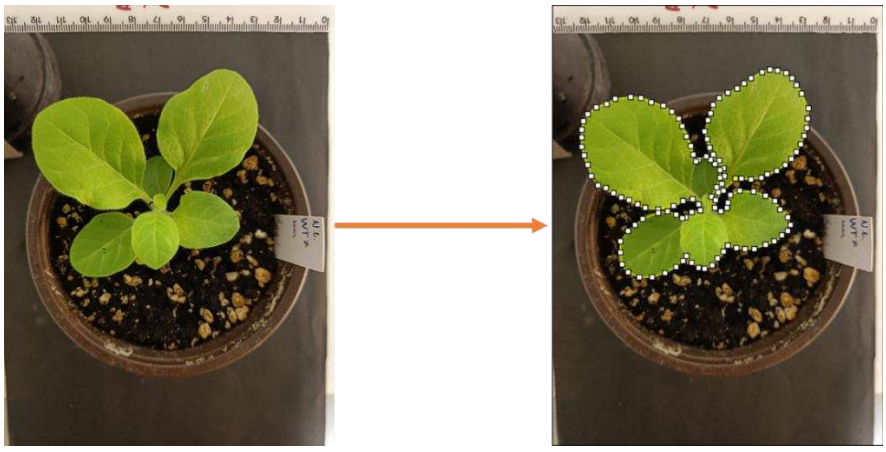

Fig. 3.4 – Canopy surface estimation with ImageJ. Plants were photographed from above and a ruler, positioned at the same height as the pot border, was used as a length reference for the estimation of the surface.

4. Results and discussion

The results will be structured as a plant transformation and phenotypic characterization pipeline. In this project the work was carried out with different plants and at different stages, but it enables to cover all phases, starting from the preparation of the expression vectors for *Hordeum vulgare* to the generation of FLV-expressing *Solanum lycopersicum* plants and to the characterization of FLV-expressing *Nicotiana tabacum* T2 plants.

4.1 Preparation of plasmids for the expression of FLVs in *H. vulgare*

Barley (*Hordeum vulgare*) is an important crop, and like many other plants of commercial interest it is a monocot. To test whether the presence of FLVs could improve the light use efficiency in barley, a new expression system had to be designed to account for the impossibility of using the expression system used in *N. tabacum* and *S. lycopersicum* as it relies on the efficient functionality of the 2A self-cleaving peptide from the foot-and-mouth disease virus, which is not optimized to function in barley and may not ensure the correct expression stoichiometry of both *flv* genes.

Flv genes from the construct used by Yamamoto, H. *et al.* (2016) [30] were separately amplified through primer couples carrying recognition sites for restriction enzymes (Fig. 4.1) and, as part of this work, were subsequently inserted into their respective sub-cloning vectors to put both genes under the control of a ubiquitin promoter (P_{Ubiq1}).

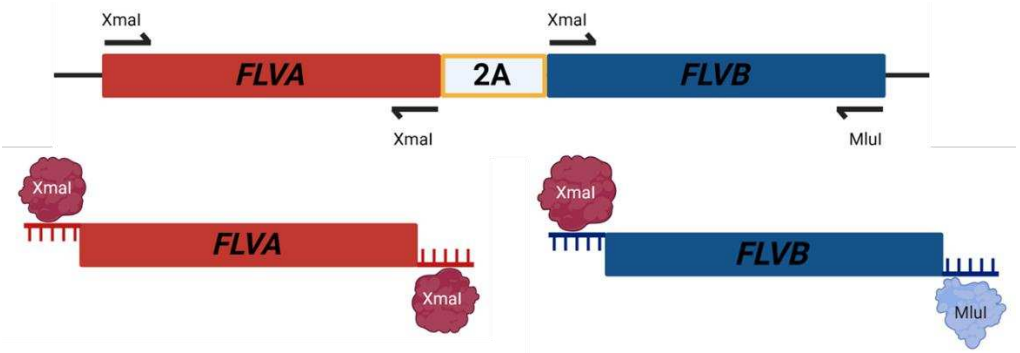

Fig. 4.1 – Schematic representation of the preliminary amplification of both *flv* genes using primers provided with endonuclease recognition sites. PCR products were purified and subjected to endonuclease activity in order to be inserted into the sub-cloning vector.

The sub-cloning vector CPGE_VEC00103_Ubi1::Flv(A/B), for both *flvA* and *flvB*, was successfully obtained and verified through restriction analysis (Fig. 4.2a; 4.2c). Numerous attempts were then done to generate the final construct, in which *flvA* and *flvB* genes are under the control of P_{Ubiq1} (Ubi1::FlvA/B), into the final expression vector CPGE_VEC00113. To do this, both Ubi1::FlvA and Ubi1::FlvB constructs had to be excised from the sub-cloning vector through the use of SfiI and ligated, without directionality, with the dephosphorylated expression vector.

The final expression vector, CPGE_VEC00113, is designed for the transformation of *A. tumefaciens* and for the subsequent Agrobacterium-mediated transformation of barley plants (4.2b). Despite the efforts, no final expression vector has been obtained yet due to the inefficient insertion of the Ubi1::Flv(A/B) construct, which is ≈4000bp-long for both genes, into the expression vector, which is ≈10000bp. This was probably due to the dimensions of both constructs and of the final vector, which decreases the efficiency and requires an optimization of the standard cloning protocol (e.g. increased dephosphorylation time with different arctic phosphatase and vector concentrations, different insert/vector ratios during ligation).

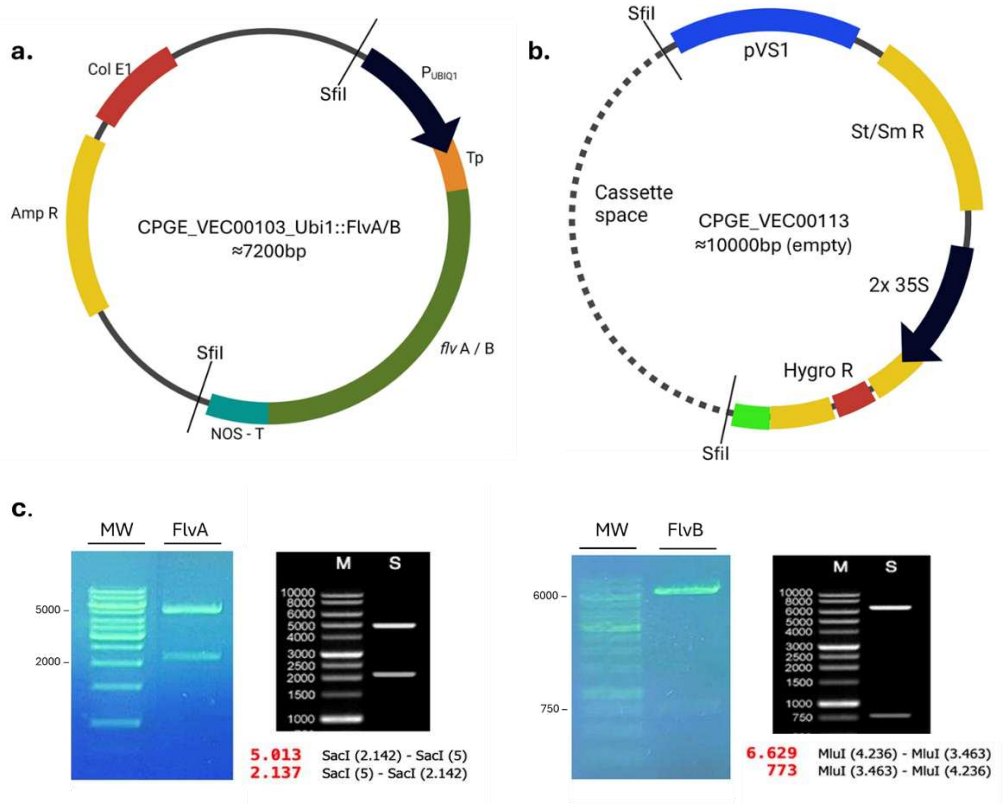

Fig. 4.2 – a) Schematic representation of the sub-cloning vector CPGE_VEC00103 with the *flv* insert and with highlighted SfiI restriction sites. b) Schematic representation of the final expression vector CPGE_VEC00113 with highlighted SfiI restriction sites and cassette space. c) Verification of the successful obtainment of both sub-cloning vectors CPGE_VEC00103_ Ubi1::FlvA and CPGE_VEC00103_ Ubi1::FlvB through restriction analysis.

4.2 Generation of *S. lycopersicum* plants expressing FLVs

One of the three main goals of this thesis was to increase the number of available FLV-expressing *Solanum lycopersicum* (tomato) lines to ensure robustness to subsequent experimental characterization of the plants. To this aim, Agrobacterium-mediated transformation was performed on 8 days-old *S. lycopersicum* cotyledons as specified in section 3.2.1. First, *Agrobacterium tumefaciens* LBA4404 was transformed with the pBinAR_35S::FlvA2AFlvB

vector (see section 3.5.1) and the success of the transformation was checked through colony PCR (Fig. 4.3) performed with the primer couple 35S Forward – FlvB seq rev 1 (predicted dimensions ≈2800bp, see Table 4).

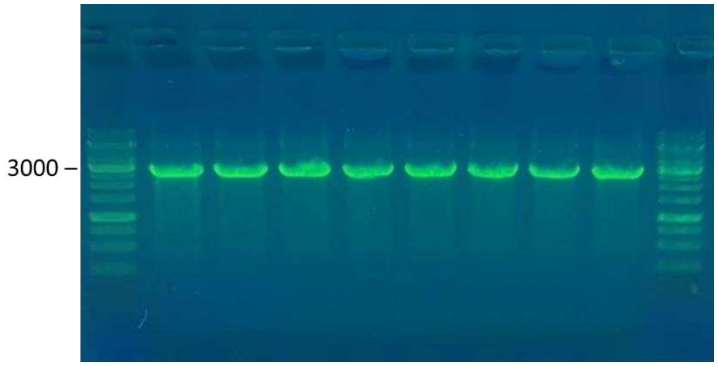

Fig. 4.3 – Agarose gel electrophoresis of a colony PCR executed on single colonies of *A. tumefaciens* transformed with the desired vector.

426 cotyledons were transformed and handled as specified in section 3.2.1. Due to bacterial contamination, which probably occurred during the transfer of the transformed cotyledons into new medium, most of the material was lost. Of the initial 426, only four cotyledons successfully de-differentiated into calluses and formed shoots (Fig. 4.4).

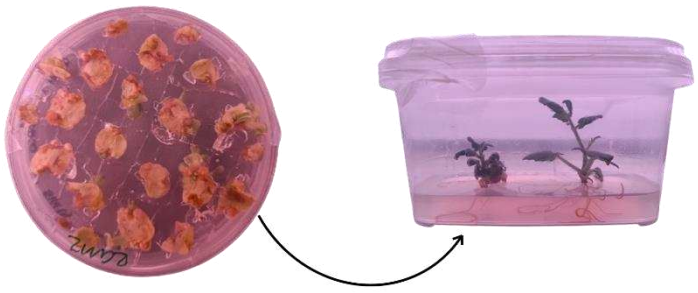

Fig. 4.4 – Once in RGM2, cotyledons dedifferentiate and start the formation of shoots. Shoots are then cut and transferred in RM to form roots and are then transferred to soil for screening and growth.

The shoots were cut and transferred in the rooting medium. Once fully developed, plantlets were transferred to soil. Once tomato plants were grown enough for a leaf to be detached, they were all screened for FLV activity at the Dual-PAM 100 through the dark-to-light P700 redox kinetic protocol. As specified in section 3.6.1, the dark-to-light P700 redox kinetic protocol consists in subjecting dark-acclimated photosynthetic samples (e.g. leaves) to a dark-to-light transition to measure the redox state of P700. In all photosynthetic samples the dark-to-light transition causes a rapid surge in the amount of oxidized P700, which is also rapidly reduced, and this type of kinetic can indeed be observed in WT plants during a dark-to-light transition (Fig. 4.5a, blue line). Instead, when FLVs are present, a slower P700 oxidation is measured right after the SP-induced P700 oxidation and subsequent reduction (Fig. 4.5a, dark green line).

Only one plant showed a P700 re-oxidation phenotype that can be associated with FLVs activity, whereas all the other plants were indistinguishable from the WT (Fig. 4.5a).

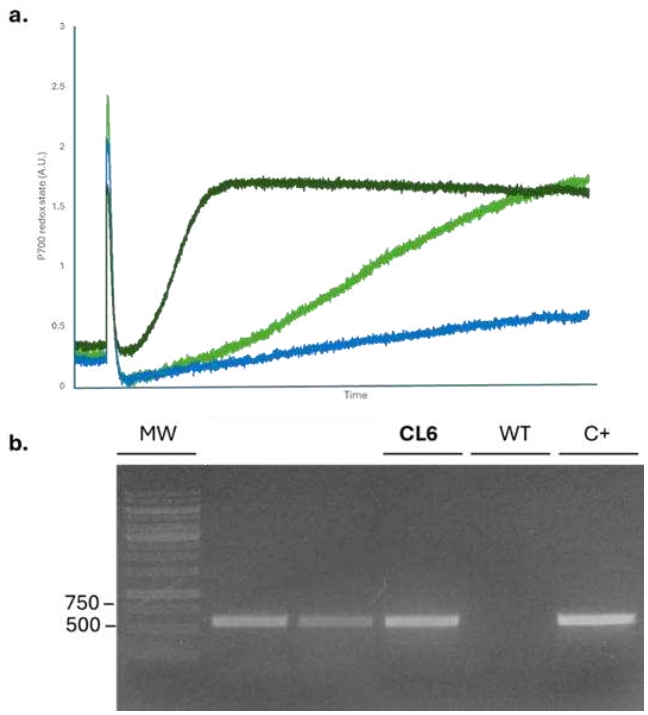

Fig. 4.5 – a) P700 redox kinetics upon a dark-to-light transition. The blue line is the P700 redox kinetic of a WT plant, the dark green line is that of a T2 *N. tabacum* plant and the light green line is that of the plant obtained by the transformation.
b) PCR on the gDNA of the tomato plant obtained by this transformation, CL6. (C+ is a FLV T2 tobacco plant).

The P700 re-oxidation phenotype seen in the tomato plant obtained by the transformation presented here (CL6, light green line in 4.5a) can be associated with functional and sub-optimal FLV activity. In fact, the P700 re-oxidation kinetic displayed by CL6 is slow when compared to that of a FLV-expressing T2 *N. tabacum* plant (Fig. 4.5a, blue line) as well as from that of a FLV-expressing T2 *S. lycopersicum* plant (See Supplementary Materials, Fig. S5).
This difference could be due to a lower degree of FLV expression in CL6 compared to the level of expression of a second-generation plant expressing FLVs.
The genomic DNA of the FLV-expressing plant was extracted, and a PCR was performed in order to check for the presence of the FLV-carrying construct (primers: 35S Forward – FlvA seq rev, predicted dimension ≈600bp, Fig. 4.5b, see Table 4). The CL6 FLV-expressing tomato plant will be self-crossed for two generations (T0 and T1) to obtain T2 plants with a more stable FLV expression. T2 plants will then be genotyped and the effects of FLV expression on photosynthesis and growth will be assessed. Since the transformation of *Solanum lycopersicum* was unsuccessful in generating a number of transgenic plants high enough, the transformation has to be repeated to obtain at least three independent FLV-expressing lines.

4.3 Genotyping of second-generation *N. tabacum* plants expressing FLVs

Seeds of several lines of T2 *N. tabacum* plants expressing FLVs were already present in the laboratory. As part of the characterization of FLV-expressing plants, 3 independent FLV-expressing lines (FLV1, FLV7 and FLV8) were chosen for genotyping. Approximately 200 T2 seeds per line were sown in ½ MS added with kanamycin in order to be selected by antibiotic resistance. As a control, two T3 *N. tabacum* lines expressing the same kanamycin resistance with no growth phenotype were used, and results are shown in Table 10.

Table 10.

	LINE	N seeds	N germinated	N resistant	% r/g
T2	1	191	178	118	66,3%
	7	205	182	133	73,1%
	8	211	198	175	88,3%
T3	35S::GUS-GFP	206	181	174	96,1%
	35S::Lhg4	218	184	167	90,7%

Each FLV line showed different proportions of kanamycin resistant seeds in respect to the number of germinated seeds, with the average value being approximately 75%. This number is consistent with the hypothesis that T2 plants are the result of a cross between heterozygous plants, as it perfectly matches the expected proportion of individuals showing the phenotype under the Mendelian Law of Segregation of genes.

Of the kanamycin-resistant plantlets, 75 for each line were transferred to soil, and only a fraction of them survived the transfer. Each plant was screened both through PCR performed on genomic DNA, to assess for the presence of the construct, and through the dark-to-light P700 redox kinetic protocol performed with the use of the Dual-PAM 100, to assess for FLV activity (Fig. 4.6a, 4.6b, Supplementary Materials Fig. S1)

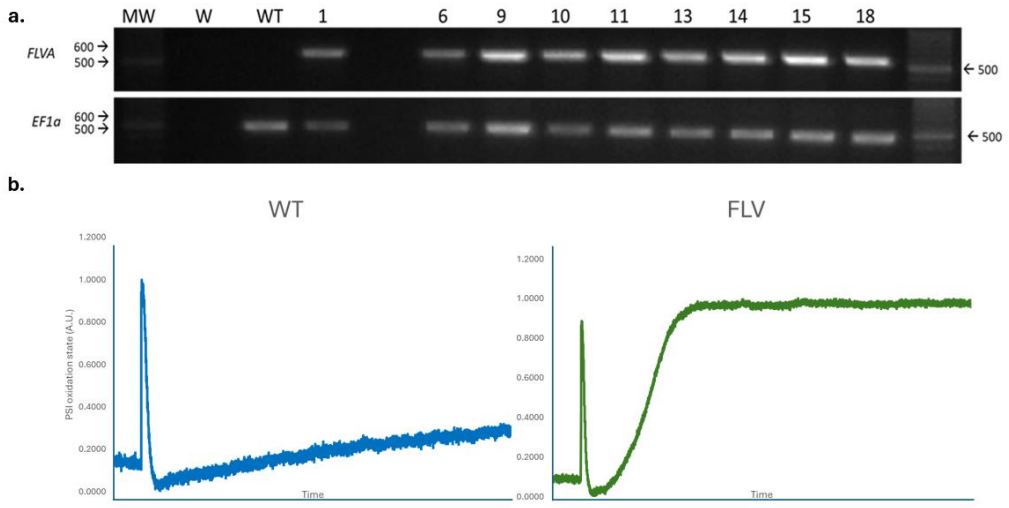

Fig 4.6 – a) Example of agarose gel electrophoresis of the PCR performed on the gDNA extracted from an FLV-expressing *N. tabacum* line (FLV1). The housekeeping gene *EF1α* was used as a control. b) Example of the results seen during the screening of plants through the dark-to-light P700 redox kinetic protocol. Plants were considered FLV-positive only when they displayed a fast P700 re-oxidation during the exposure to saturating light and were considered negative when similar to a WT P700 kinetic.

All kanamycin-resistant plants that survived the transfer in soil were also positive for the presence of the FLV-carrying construct, tested through PCR, proving correct integration and stable inheritance of the transgenes. Of these plants, over 90% for all three lines (FLV1 = 93%, FLV7 95%, FLV8 100%) were also positive for FLV activity. Overall, these results suggest that T2 *N. tabacum* plants are the result of the crossing between T1 plants that were heterozygous for the presence of the FLV-carrying construct. Therefore, 33% of the kanamycin-resistant plants are homozygous and 66% are heterozygous for the presence of the FLV-carrying construct. The fact that not all the PCR-positive plants show FLV activity could be due to individual differences in gene expression and/or protein accumulation.
Several plants were also checked for the presence of FlvB through Western Blot as a representative for correct FLVs expression (Fig. 4.7). Unfortunately, it was not possible to perform a successful Western Blot procedure for FlvA as the antibody was unsuccessful in detecting the presence of FlvA in tobacco protein extracts. The procedure was repeated with different sample and antibody concentrations as well as with different types of gel (e.g. added with urea) but no FlvA signal could be detected.

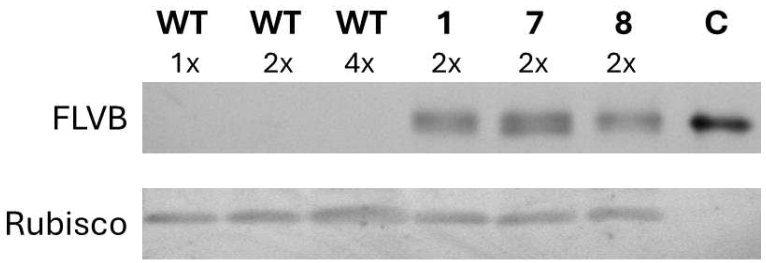

Fig. 4.7 – Example of a Western Blot targeting FlvB. Rubisco was used as a control. The "C" (control) lane was loaded with a purified FlvA and FlvB mixture.

FLV plants were also checked for alterations in the accumulation of proteins of the photosynthetic apparatus involved in LEF and in carbon fixation (Fig. 4.8). The results suggest that FLVs presence does not significantly affect the expression and accumulation of other proteins involved in photosynthesis.

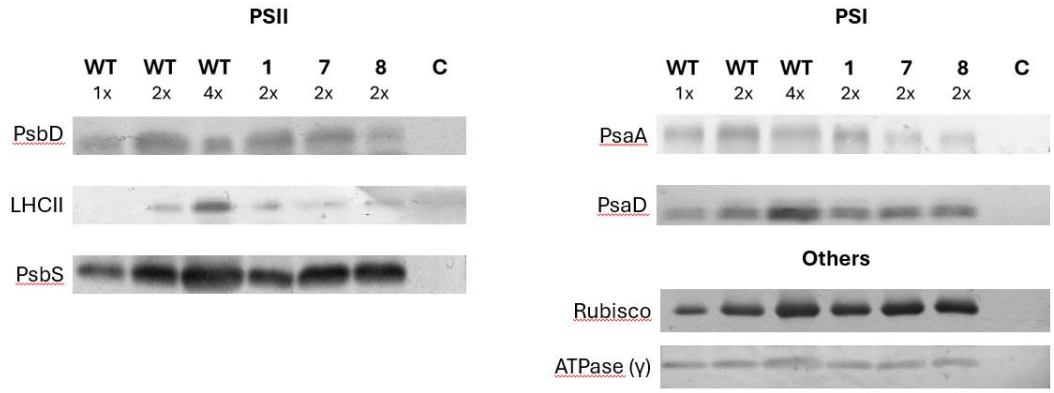

Fig. 4.8 – Results of Western Blotting procedures targeting major components of the photosynthetic machinery.

4.4 FLVs are functional in *N. tabacum* with profound consequences

The main objective of this thesis project was to characterize the consequences of FLVs expression on the photosynthesis of angiosperms, of which *Nicotiana tabacum* is a model organism. Once T2 *N. tabacum* FLV plants were fully genotyped, adult plants were screened using both the Dual-PAM 100 and the JTS-10.

To quantitatively measure the effects of FLV expression i*n vivo* the rSP protocol was applied, which indeed allows for the quantification of the $P700^+$ proportion of the total P700 reaction centres in the sample (see section 3.6.3). The protocol consists of six saturating pulses supplied after an initial one (used to measure the P_m) in the presence of the desired actinic light background of 70µE. Each pulse causes a spike in the oxidation state of P700 as a result of the SP-induced oxidation of open P700 RCs, and the area under the last spike is calculated for $P700^+$ estimation (Fig. 4.10a; 4.10b), following the principles specified by Klughammer & Schreiber (2008).

The results indicate that FLVs expression drastically increases the $P700^+/P700$ ratio in respect to WT, proving that FLVs act as efficient electron sinks downstream of PSI upon rapid and drastic increases in light intensity. When considering this finding in relation to what has been observed by Sejima *et al.* (2014) in sunflower leaves, it appears that FLVs expression may be able to prevent PSI photoinhibition during saturating pulses even with low background actinic light. In the mentioned paper the authors applied the rSP protocol, with increasing background actinic light intensity, to sunflower leaves. Thanks to this approach the authors were able to see that the $P700^+/P700$ ratio increases along with the increasing of the background actinic light, and also observed that the percentage of PSI photoinhibition (measured through the decrease in P_m after the rSP protocol) is the highest when the $P700^+/P700$ ratio is the lowest, highlighting the protective effects of P700 oxidation against photoinhibition (4.10c). In the mentioned paper, the $P700^+/P700$ ratio at low background actinic light (200µE) measured in WT sunflower leaves is similar to the $P700^+/P700$ ratio of WT tobacco plants in

this work, with 70μE of background actinic light. On the other hand, the $P700^+/P700$ ratio measured in FLV plants with 70μE of background actinic light is higher than that measured by Sejima *et al.* in sunflower leaves at 1400μE. Thus, the rSP data gathered as part of this work, along with the evidence produced by Sejima *et al.*, suggest that the presence of FLVs maintains the P700 pool in a mostly oxidized state, protecting it from photoinhibition.

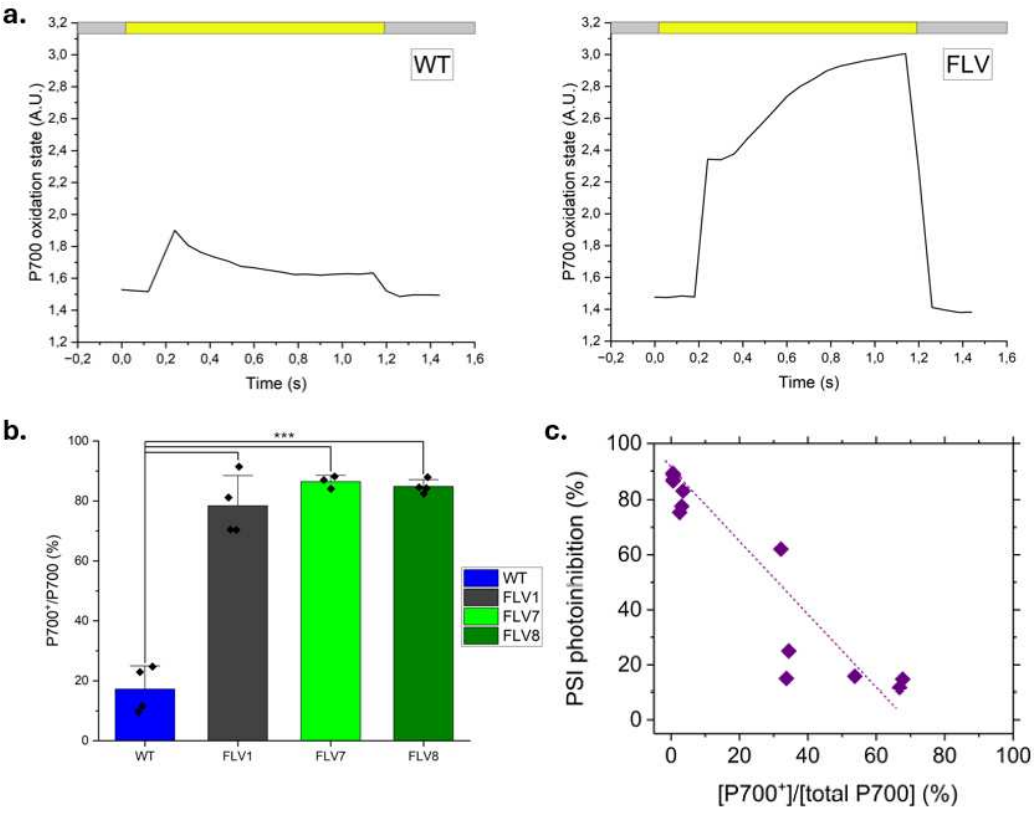

Fig. 4.10 – a) Plots depicting examples of the P700 redox kinetics during the last pulse of a rSP experiment for both WT and FLV plants. The area under the peak is an indicator of the number of oxidized P700 reaction centres. b) Comparison of the $P700^+/P700$ ratio of WT and FLV plants as measured through the rSP protocol. N=4, the statistical analysis was performed through the Student's *t*-test (*: 0.05>p>0.01; **: 0.01>p>0.001; ***: p<0.001). c) Decrease in photo oxidable P700 (P_m) plotted against the $P700^+/P700$ ratio, from Shimakawa, G. & Chikahiro, M. (2018).

Another light protocol that was applied was the fluctuating light protocol (see section 3.6.2) in order for energy conversion efficiency at both PSII and PSI to be measured (Fig. 4.9). The fluctuating light protocol consists of 3 cycles, with each cycle consisting of 5 minutes of low actinic light and 1 minute of saturating light.

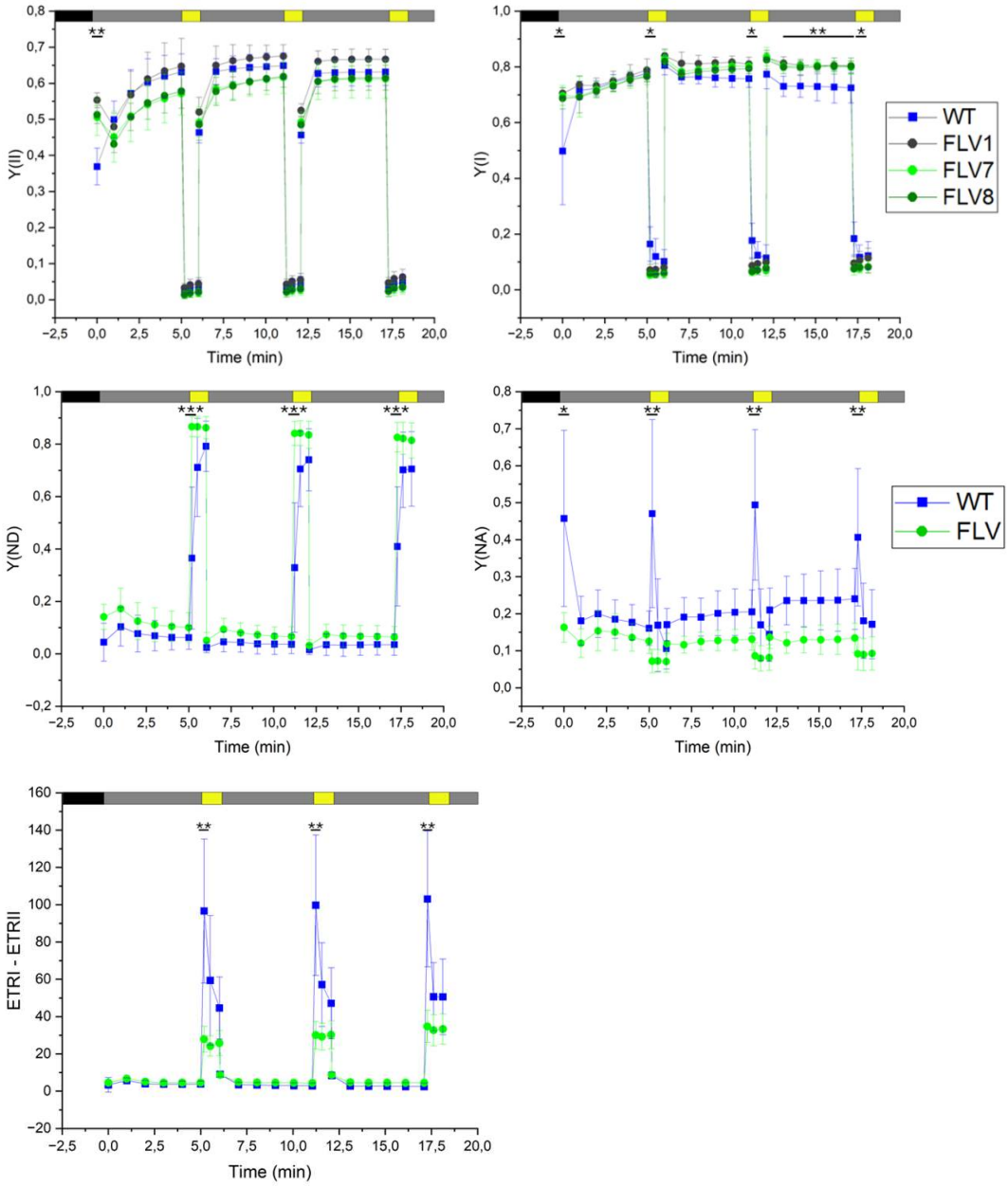

Fig 4.9 – Results of photosynthesis measurements performed with the fluctuating light protocol through the Dual-PAM 100. The first two graphs show quantum yield of PSII and PSI as WT vs all three FLV lines. Since the trend of the three FLV lines was similar, their data were merged to simplify the statistical analysis and for better visualization. $N(\mathrm{WT}) = 6$; $N(\mathrm{FLV}) = 17$. Each point is a mean $\pm$ *s.d.*
Statistical analysis was performed through the Mann-Whitney non-parametric test (*: 0.05>p>0.01; **: 0.01>p>0.001; ***: p<0.001).
(Y(ND): PSI donor-side limitation; Y(NA): PSI acceptor-side limitation; ETRI-ETRII: difference between the electron transport rate at PSI and that at PSII).

When the low actinic light is switched on for the first time (when plants are still dark-acclimated) significant differences can be measured in the photochemical quantum efficiency of both photosystems, Y(II) and Y(I), with FLV plants showing higher values in both cases. No other substantial

differences were measured regarding Y(II), but in the first seconds after low-to-high light transitions WT plants appear to have a slightly greater Y(I) in respect to FLV plants. On the other hand, FLV plants show higher Y(I) during low-light periods.

Two other fundamental parameters are Y(ND) and Y(NA), which are the donor and acceptor side limitations of PSI, respectively. During the light protocol, FLV plants maintain a slightly higher PSI donor side limitation, and this difference become significant in the first twenty seconds after a low-to-high light transition, meaning that FLVs maintain the P700 pool in an oxidized, donor side-limited state. Consistent with this, FLV plants show a constantly lower Y(NA) in respect to WT plants. In fact, during low-to-high light transitions, WT plants show a much greater acceptor side limitation than FLV plants, proving that FLVs presence prevents the over-reduction of the electron transport chain downstream of P700, also confirming what was previously seen by other research groups. These data show how the expression of FLVs prevents acceptor-side limitation of PSI, which is instead donor-side limited in the first seconds after the sudden increases in light intensity in FLV plants. Taken together, these results suggest that FLVs are fully functional in *Nicotiana tabacum* by acting as an electron sink downstream of PSI that prevents its acceptor side limitation. Moreover, the data show that the expression of FLVs does not significantly alter the photochemical quantum efficiency of PSII at the steady state but does increase that of PSI.

The fact that the Y(I) of FLV plants is increasingly higher than that of WT plants during the light protocol could be due to FLVs being capable of preventing PSI photoinhibition after repetitive low-to-high light transitions.
This correlates well with Y(NA) data, which show that FLVs expression limits the acceptor-side limitation of PSI caused by the over-reduction of the photosynthetic electron transport chain during sudden increases in light intensity. Indeed, it can be seen that the Y(NA) parameter of WT plants is increasingly greater than that of FLV plants during the light protocol. One interesting parameter to be accounted for is the difference between the electron transport rates of PSI and PSII (ETRI-ETRII), which is an indicator of cyclic electron flow around PSI. Upon sudden increases in light intensity, WT plants display a high ETRI-ETRII in respect to FLV plants, which is consistent with the hypothesis that FLVs expression competes with alternative electron flows like CEF. Indeed, while CEF cycles electrons from the acceptor side of PSI to its donor side, the pseudo-CEF mediated by FLVs redirects electrons from the photosynthetic electron transport chain to the reduction of oxygen. Because of this, FLVs presence could explain the difference in ETR between the two photosystems in the two genotypes.

To fully understand the effects of FLVs expression on the photosynthetic electron transport rate (ETR), the Xenon and DIRK protocols (see section 3.7) were applied through the JTS-10 to perform ECS measurements on dark-acclimated WT and FLV plants grown in control conditions. The Xenon protocol was used to measure the amount of PSII+PSI present in the illuminated portion of the sample, which was used as a normalization factor for the ECS signal measured through the DIRK protocol.
The difference between the ECS signals measured before and after each "dark interval" provides a measure of the ETR (Fig. 4.11a; 4.11b, see section 3.7).
ECS signals at 520nm were corrected for scattering-induced optical changes by subtracting the ECS signal measured at 546nm.

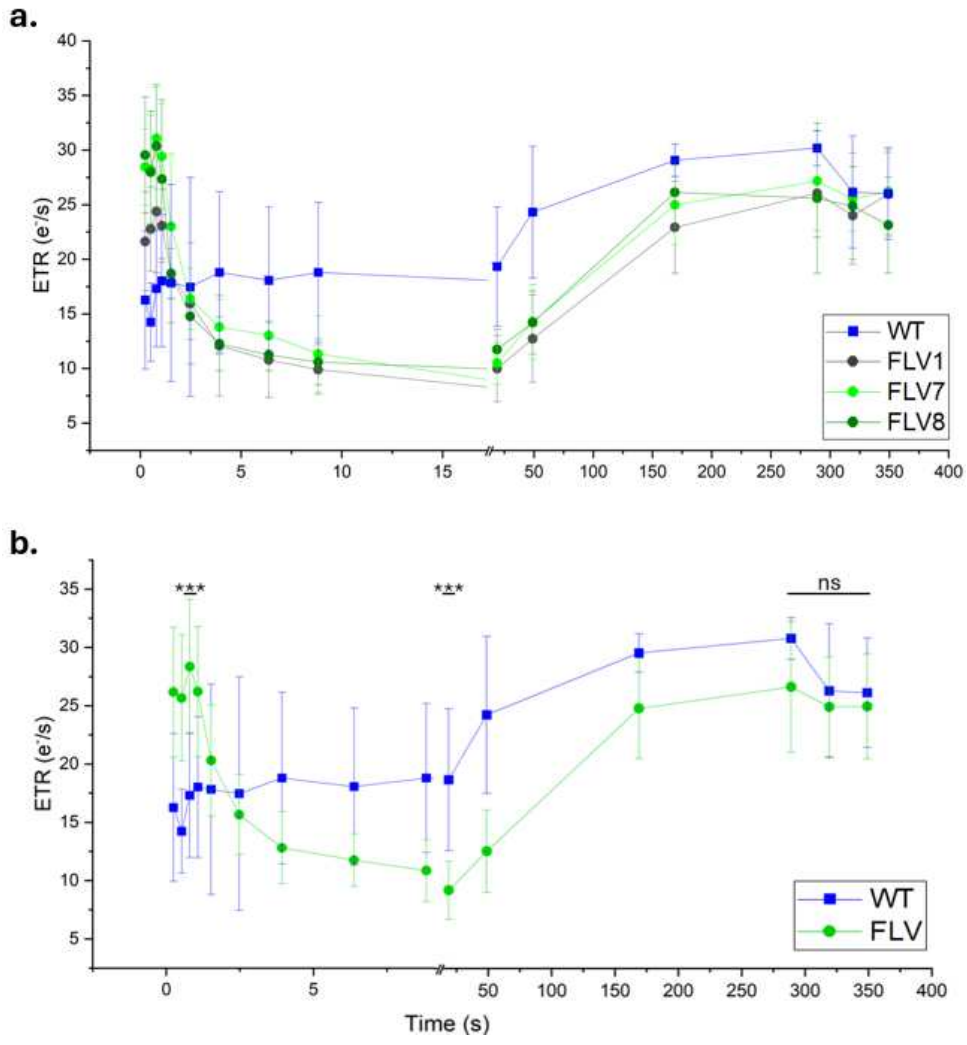

Fig. 4.11 – a) ETR vs time plot of all independently shown FLV lines and of WT plants. $N \geq 5$, each point is a mean $\pm$ *s.d.* b) ETR vs time plot in which ETR values of FLV plants were calculated as the average between all the plants of all three independent lines to simplify both visualization and data analysis. Statistical analysis was performed through the Mann-Whitney non-parametric test (*: $0.05>p>0.01$; **: $0.01>p>0.001$; ***: $p<0.001$; ns: non-significant).

In the first seconds after the onset of the actinic light (500μE) WT individuals show a relatively stable ETR that starts rising only after approximately 20 seconds, and by the end of the illumination period (300s) the ETR has almost doubled the initial value. FLV-expressing plants, on the other hand, show a peak in ETR in the first 3 seconds after the onset of actinic illumination, which is likely the result of FLVs being active as electron sinks downstream of PSI. Interestingly, the ETR of FLV plants drops to almost half of that of WT individuals between 4 and 50 seconds after the onset of actinic illumination and reaches the same values as WT plants only by the end of the illumination period, when photosynthesis is at the steady state. Overall, these results suggest that, in the first seconds after light is switched on, the ETR in WT individuals is limited by the acceptor-side limitation of PSI, which is instead relieved by the presence of FLVs in FLV plants. Instead, after 5 seconds of illumination, WT plants show greater ETR than FLV plants, suggesting that a slower-inducing alternative electron transport mechanism is active in WT individuals but not in FLV plants. At the steady state, when leaves are completely light-adapted and the CBB cycle is fully induced, no differences between WT and FLV plants can be seen.

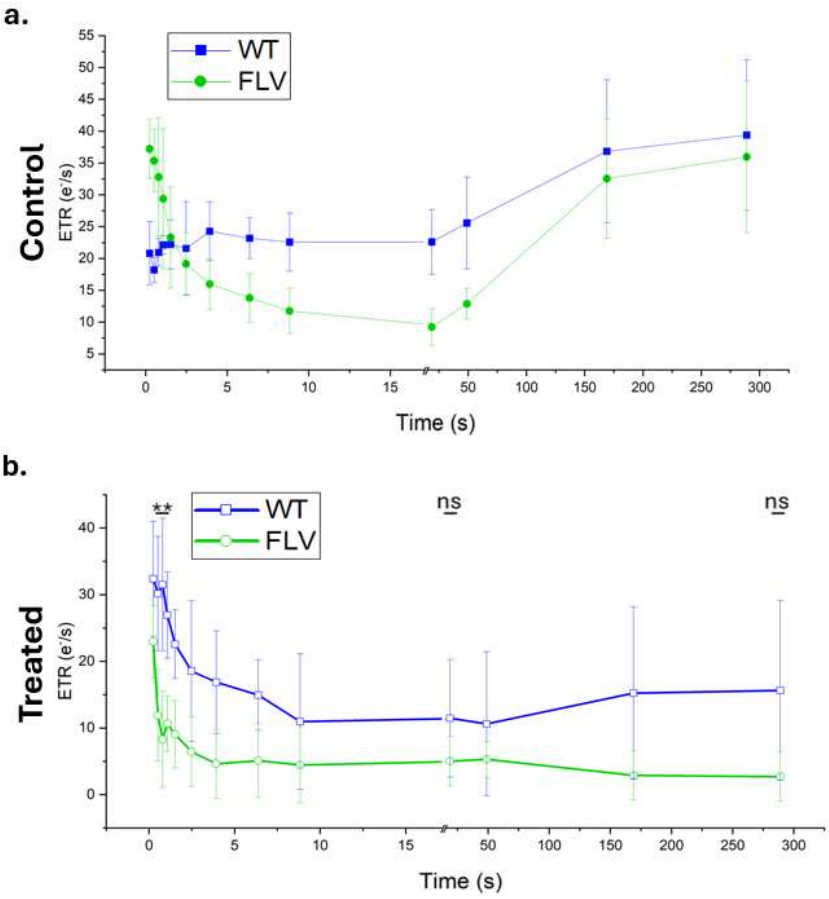

Fig. 4.12 – a) ETR measurements carried out in control conditions. The similarity between these results and those performed with still-attached leaves proves that the measurements performed with leaf samples are biologically consistent. b) ETR measurements after 1h-long DCMU treatment. $N(\mathrm{WT}) = 5$; $N(\mathrm{FLV}) = 17$. Statistical

analysis was performed through the Mann-Whitney non-parametric test (*: 0.05>p>0.01; **: 0.01>p>0.001; ***: p<0.001; ns: non-significant).

Both these results and the results gathered through Dual-PAM 100 measurements point out to a different activation of cyclic electron flows between WT and FLV plants, in which FLVs are likely to compete for the electrons at the acceptor side of PSI. To determine whether this could be due to FLV-mediated pseudo-CEF competing with CEF, the same measurements at the JTS-10 were performed on dark-acclimated leaf samples treated with DCMU as specified in section 3.7.1 (Fig. 4.12a; 4.12b). As a control, leaf samples of the same size were treated with water for the same time as the DCMU-treated ones. After the 1h-long DCMU treatment, the peak in ETR displayed by FLV plants in control conditions cannot be measured, and the ETR after less than 5 seconds from the onset of illumination is drastically lower than that measured in control conditions. On the other hand, in the same period, DCMU-treated WT plants display an ETR trend that is like that of control FLV plants, with a peak in the first seconds after the light is switched on. Interestingly, the initial value of ETR in DCMU-treated WT plants appears to be higher than that of plants in control conditions. Halfway through the light protocol and at the end of it, at the steady state of photosynthesis, the ETR values of both WT and FLV individuals are approximately 25% of those measured in control conditions and do not show significant differences between them. This proves that DCMU is successfully inhibiting PSII, which only shows residual activity, thus limiting the LEF in both genotypes. DCMU is an inhibitor of PSII and thus it blocks the linear electron flow from PSII to Cyt b_6f and to PSI. Therefore, the ETR measured in presence of DCMU is mostly due to the activity of alternative electron flows around PSI, and in angiosperms the main alternative pathway is CEF. Considering this, these data point out that when FLVs are present they compete with CEF in *N. tabacum* during the first seconds after actinic illumination is switched on, and in fact they appear to limit its induction. If CEF and FLV-mediated pseudo-CEF did not compete, and if FLVs presence did not affect CEF, no difference between WT and FLV plants would be measured after DCMU treatment in the first seconds after the onset of illumination.
To determine whether these differences could be due to a different expression or accumulation of proteins involved in CEF, proteins from WT and FLV plants were extracted and subjected to Western Blot procedures (Fig. 4.13).

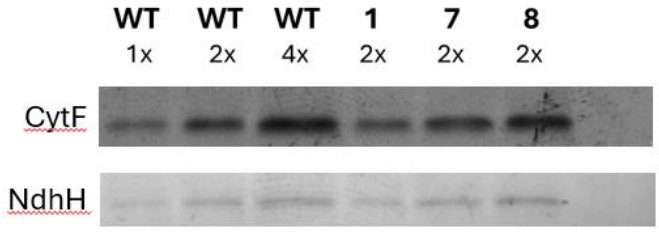

Fig. 4.13 – Results of Western Blotting procedures targeting CytF, a subunit of the Cyt b_6f complex, and NdhH, a subunit of the NDH complex which is involved in CEF around PSI.

The results of the performed Western Blots, although not targeting all the putative molecular effectors of CEF, do not highlight substantial differences in the accumulation of the targeted proteins, suggesting that FLVs presence does not alter the accumulation of proteins and complexes involved in alternative electron flows but rather impact their activity *in vivo*.

4.5 Plants expressing FLVs are less sensitive to fluctuating light

The results presented in this thesis, as well as the results of other studies, converge on the conclusion that, when present, FLVs are active in contributing to the photosynthetic electron transport chain downstream of PSI and in limiting its acceptor-side limitation during sudden light intensity increases.
To test whether FLVs presence protects PSI from photoinhibition and confers resistance to strong, cyclic fluctuations in light intensity, *N. tabacum* WT and FLV plants were grown for 14 days under fluctuating light conditions. Treated plants were grown at 16°C and with a photoperiod of 16 hours of light and 8 hours of darkness (see section 3.8). During the light period, plants were exposed to 50µE for 4.5 minutes followed by 30 seconds at 1000µE. Control plants were grown in the growth chamber (see conditions in section 3.1). The experiment was performed three independent times with 3 weeks-old plants. The Fv/Fm of both control and treated plants was measured daily. The P_m was measured daily only on a subset of plants subjected to growth under fluctuating light (Fig. 4.14; control data in Supplementary Materials Fig. S2).

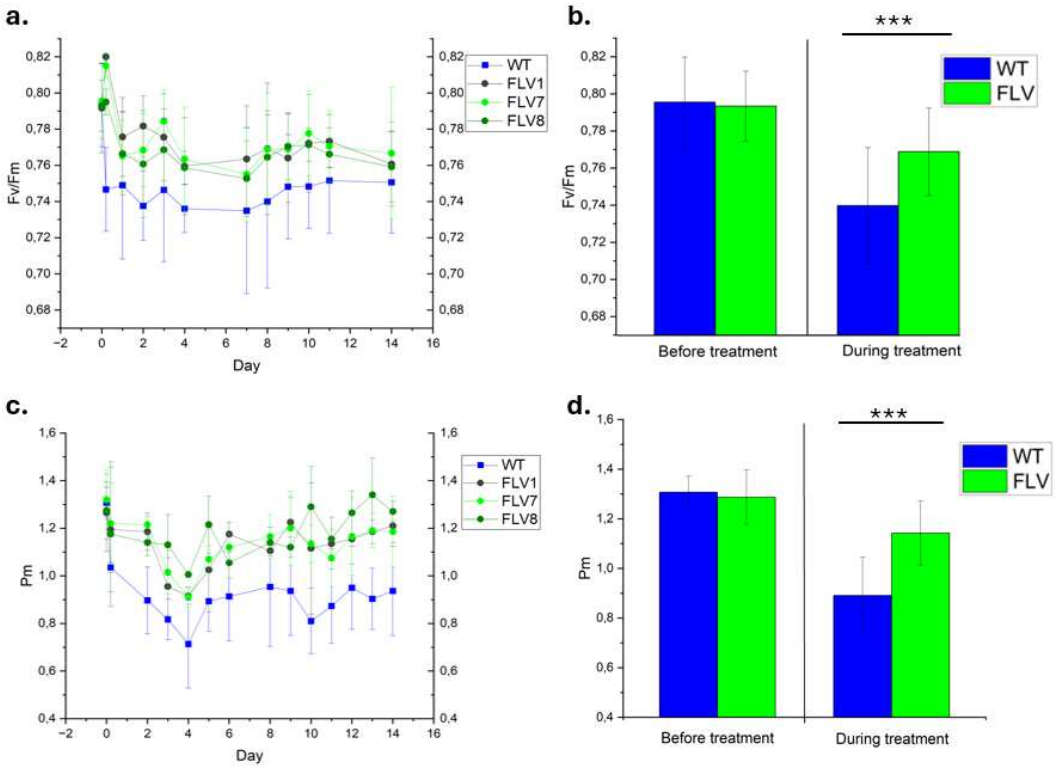

Fig. 4.14 – a) Daily Fv/Fm values of WT and FLV plants grown under fluctuating light. *N*(WT)=7, *N*(FLV)=6. Data are presented as mean ± *s.d.* b) Comparison between

average Fv/Fm data measured before the period of growth under fluctuating light and during the whole period of growth, presented as the average of all the values measured from day 1 to day 14. Data are presented as mean ± *s.d.* Statistical analysis was performed through the Student's *t*-test (***: p<0.001).
c) Daily Pm values of WT and FLV plants grown under fluctuating light. N(WT)=3, N(FLV)=2. Data are presented as mean ± s.d. d) Comparison between average Pm data measured before the period of growth under fluctuating light and during the whole period of growth, presented as the average of all the values measured from day 1 to day 14. Data are presented as mean ± *s.d.* Statistical analysis was performed through the Student's *t*-test (***: p<0.001).

The Fv/Fm ratio is the maximal quantum efficiency of PSII and it is interpreted as a general indicator of the plant's well-being that decreases in presence of stress. *N. tabacum* plants grown in control conditions have an Fv/Fm value that oscillates around 0.8 (see Supplementary Materials Fig. S2) for both WT and FLV individuals. Considering this, the Fv/Fm data gathered over a two-week period of growth under fluctuating light prove that the treatment is stressful and effectively decreases the Fv/Fm ratio of the treated plants, of both genotypes. Still, FLV-expressing plants show a constantly and significantly higher Fv/Fm over the whole two-weeks period in respect to WT individuals. Although with fewer replicates, these results are mirrored by the P_m parameter, which can instead be interpreted as the maximal photo-oxidable P700 and its decrease is a symptom of PSI photoinhibition. Overall, these data suggest that the photosynthetic machinery of FLV-expressing *N. tabacum* plants is less sensitive to growth under fluctuating light in respect to WT plants. To determine whether this decreased photosynthetic sensitivity translates in increased biomass production the canopy surface of each plant, both control and treated, was measured once every three days (Fig 4.15a; Supplementary Materials Fig. S3). At the end of the treatment, the aerial part of each plant was collected and dried as specified in section 3.8 (Fig. 4.15b, Supplementary Materials Fig. S4). The results do not take into consideration the canopy surface and the dry weight of plants of the third repetition of the experiment due to incompatibility between data, likely caused by a change in the soil composition.

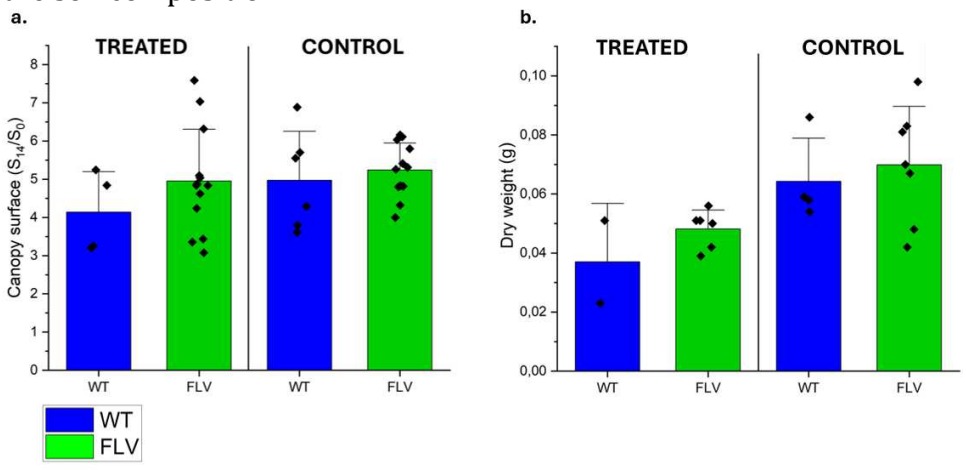

Fig. 4.15 – a) Canopy surface of WT and FLV plants, both treated and control, expressed as the ratio between the surface measured at day 14 and that measured at day 0. b) Dry weight values of WT and FLV plants, both treated and control, taken during the first repetition of the experiment. The rest of the data is shown in Supplementary Materials, Fig. S4.

Plant growth is a complex and multifactorial parameter that can be estimated through different approaches and requires expertise to be fully characterized and interpreted. Although the results appear to be non-significant, by taking into consideration the average values, the distribution of canopy surface, weight values and the phenotypic appearance of the plants (see Supplementary Materials, Fig. S3), it can be stated that FLV plants tend to grow more than WT plants under fluctuating light conditions at 16°C.

4.6 Conclusions

One of the objectives of this thesis was the generation of an FLVs expression system for barley. *Flv* genes were independently amplified, starting from the FLV-carrying construct used for FLVs expression in both *N tabacum* and *S. lycopersicum*, and cloned within a sub-cloning vector (CPGE_VEC00103). The step in the sub-cloning vectors was necessary to put both genes under the control of the desired promoter (P_{Ubiq1}), and both sub-cloning vectors were successfully obtained. The next step, which is still ongoing, is the successful generation of the expression vectors and subsequent transformation of *H. vulgare*, to which follows the pipeline presented in this work.

The secondary objective of this work was the generation of at least two independent *S. lycopersicum* lines expressing FLVs through Agrobacterium-mediated transformation. Due to the time required for one transformation to produce transgenic and adult plants (3-4 months), and due to contamination, only one adult FLV-expressing *Solanum lycopersicum* plant was obtained as part of this work. Although less than planned, the FLV-expressing line obtained during this thesis project adds to the ones already present in the laboratory. The study of the effects of FLVs expression in *S. lycopersicum* is an important part of the research on FLVs because tomato is a model organism for fruit development. Because of this, the FLV-expressing tomato line obtained as part of this thesis project represents one step further to the characterization of the effects of FLVs on fruit development.

Most of the effort was dedicated to the in-depth characterization of FLV-expressing *Nicotiana tabacum* plants, which has provided several meaningful insights on how they affect the photosynthetic electron transport: FLVs are functional in *N. tabacum*, where they efficiently prevent PSI acceptor-side limitation during rapid transitions to high light intensities without affecting the efficiency of PSII or the accumulation of proteins of the major photosynthetic complexes. FLVs presence increases the $P700^{+}/P700$ ratio during saturating pulses in presence of low background actinic light, suggesting that they are capable of preventing PSI photoinhibition, and their activity competes with CEF for the electron flow downstream of PSI in the first instants after the onset of actinic illumination. Finally, FLV-expressing plants show to be less sensitive to growth under fluctuating light conditions as suggested by their photosynthetic machinery being less affected and by their increased growth and development.

FLVs appear to be a promising instrument for a deeper understanding of the mechanisms with which it may be possible to increase the efficiency of the conversion of sunlight into biomass.

Several questions still remain unanswered, such as why FLVs were lost by angiosperms during their evolution and why CEF was preserved instead, especially given the fact that their presence does not appear to negatively affect plant growth or development. In fact, the characterization of the effects

of FLVs expression in angiosperms is far from being completed. This thesis, although showing promising results, does not provide definitive evidence of undoubtedly positive effects of FLVs regarding plant growth and resistance to fluctuating light. This calls for a more statistically sound approach in which growth under fluctuating light is evaluated on a high number of individuals and by taking into account several parameters. Moreover, to test if the results obtained in this work are species-specific, the same phenotypic characterization that was done in *N. tabacum* should be done in other species (e.g. *Solanum lycopersicum* and *Hordeum vulgare*). The use of *S. lycopersicum* could be of particular interest regarding the study of the effects of FLVs expression in fruit development. Finally, since it appears that FLV-dependent pseudo-CEF competes with CEF, FLVs could be expressed in mutants in which CEF is impaired to check whether they are able to complement it.

5. References

1. Gregory, T.R. Artificial Selection and Domestication: Modern Lessons from Darwin's Enduring Analogy. *Evo Edu Outreach* **2**, 5–27 (2009).
2. Ibarra-Ross J., Morrell, P. L. & Gaut, B. S. Plant domestication, a unique opportunity to identify the genetic basis of adaptation. *PNAS* **104**, 8641-8648 (2007).
3. Salgotra, R. K. & Chauhan, B. S. Genetic Diversity, Conservation, and Utilization of Plant Genetic Resources. *Genes (Basel)* **14**, 174 (2023).
4. United Nations Department of Economic and Social Affairs, Population Division (2022). World Population Prospects 2022: Summary of Results.
5. FAO, 2021. Land use statistics and indicators statistics. Global, regional and country trends 19902019. FAOSTAT Analytical Brief Series No 28. Rome.
6. Aziz, M. A., Brini, F., Rouached, H. & Masmoudi, K. Genetically engineered crops for sustainably enhanced food production systems. *Front Plant Sci* **13**, 1027827 (2022).
7. Zhu, X., Long, S. P. & Ort, D. R. Improving photosynthetic efficiency for greater yield. *Annu Rev Plant Bio* **61**, 235-261 (2010).
8. Cardona, T., Shao, S., & Nixon, P. J. Enhancing photosynthesis in plants: the light reactions. *Essays in Biochemistry* **62**, 85-94 (2018).
9. Blankenship, R. E. Molecular Mechanisms of Photosynthesis, 3rd edition. *John Wiley & Sons Inc.* (2021).
10. Xiong, J. & Bauer, C. E. Complex evolution of photosynthesis. *Annu Rev Plant Bio* **53**, 503-521 (2002).
11. Blankenship, R. E. Early Evolution of Photosynthesis. *Plant Physiol.* **154**, 434-438 (2010).
12. Santabarbara, S., Agostini, G., Casazza, A. P. *et al.* Chlorophyll triplet states associated with Photosystem I and Photosystem II in thylakoids of the green alga *Chlamydomonas reinhardtii. Biochimica et Biophysica Acta* **1767**, 88-105 (2007).
13. Alberts, B., Bray, D., Johnson, A. *et al.* Molecular Biology of the Cell, 4th edition. *Garland Science, Taylor & Francis Group LLC* (2014).
14. Malone, L. A., Proctor, M. S., Hitchcock, A. *et al.* Cytochrome b_6f – Orchestrator of photosynthetic electron transfer. *Biochimica et Biophysica Acta* **1862**, 148380 (2021).
15. Fukuyama, K. Structure and Function of Plant-Type Ferredoxins. *Photosynthesis Research* **81**, 289-301 (2004).
16. Prywes, N., Phillips N. R., Tuck O. T. *et al*. Rubisco Function, Evolution and Engineering. *Annu Rev Bioch* **92**, 385-410 (2023).
17. Ensen, E., Clément, R., Maberly, S. C. & Gontero, B. Regulation of the Calvin-Benson-Bassham cycle in the enigmatic diatoms: biochemical and evolutionary variations on an original theme. *Philos Trans R Soc Lond B Biol Sci* **372,** 1728 (2017).
18. Bhattacharjee, S., Neese, F. & Pantazis, D. A. Triplet states in the reaction center of Photosystem II. *Chem. Sci.* **14**, 9503-9516 (2023).
19. Theis, J. & Schroda, M. Revisiting the photosystem II repair cycle. *Plant Signal Behav.* **11**, e1218587 (2016).

20. Zafaver, A. & Mancilla, C. Concepts of photochemical damage of Photosystem II and the role of excessive excitation. *Journal of Photochemistry and Photobiology* **47**, 100421 (2021).
21. Goss, R. & Lepetit, B. Biodiversity of NPQ. *Journal of Plant Physiology* **172**, 13-32 (2015).
22. Nawrocki, W. J., Bailleul, B., Picot, D. *et al*. The mechanism of cyclic electron flow. *Biochimica et Biophysica Acta*, **1860**, 433-438 (2019).
23. W. Nawrocki, B. Bailleul, P. Cardol *et al*. Cyclic Electron Flow in *Chlamydomonas reinhardtii*. *BioRxiv* (2017).
24. Alboresi, A., Sorti, M., Morosinotto, T. Balancing protection and efficiency in the regulation of photosynthetic electron transport across plant evolution. *New phytologist* **221**, 105-109 (2019).
25. Curien, G., Flori, S., Villanova, V. *et al*. The Water to Water Cycles in Microalgae. *Plant & Cell Physiology* **0**, 1-10 (2016).
26. Asada, K. The water-water cycle as alternative photon and electron sinks. *Phil. Trans. R. Soc. Lond.,* 355, 1419-1431 (2000).
27. Ilík, P., Pavlovic, A., Kouřil, R. *et al.* Alternative electron transport mediated by flavodiiron proteins is operational in organisms from cyanobacteria up to gymnosperms. *New Phytologist* **214**, 967-972 (2017).
28. Folgosa, F. Martins, M. C. & Teixeira, M. The multidomain flavodiiron protein from *Clostridium difficile* 630 is an NADH:oxygen oxidoreductase. *Nature Scientific Reports* **8**, 10164 (2018).
29. Allahverdiyeva, Y., Isojärvi, J., Zhang, P. & Aro, E. Cyanobacterial Oxygenic Photosynthesis is Protected by Flavodiiron Proteins. *Life* **5**, 716-743 (2015).
30. Beraldo, C., Traverso, E., Boschin, M. *et al*. Physcomitrium patens flavodiiron proteins form a redox-dependent heterocomplex. *BioRxiv* (2024).
31. Gerotto, C., Alboresi, A., Meneghesso, A. *et al.* Flavodiiron proteins act as a safety valve for electrons in *Physcomitrella patens*. *PNAS* **113**, 12322-12327 (2016).
32. Yamamoto, H., Takahashi, S., Badger, M. *et al.* Artificial remodelling of alternative electron flow by flavodiiron proteins in Arabidopsis. *Nature Plants* **2**, 16012 (2016).
33. Wada, S., Yamamoto, H. Suzuki, Y. *et al.* Flavodiiron protein substitutes for cyclic electron flow without competing CO2 assimilation in rice. *Plant Physiology* **176**, 1509-1518 (2018).
34. Fillatti, J. J., Kiser, J., Rose, B. *et al.* Efficient transformation of tomato and the introduction and expression of a gene for herbicide tolerance. *Proceedings of Tomato biotechnology*, 199-210 (1987).
35. Klughammer, C. & Schreiber, U. Complementary PS II quantum yields calculated from simple fluorescence parameters measured by PAM fluorometry and the Saturation Pulse methods. *PAM Application Notes* **1**, 27-35 (2008).
36. Klughammer, C. & Schreiber, U. Saturation Pulse method for assessment of energy conversion in PS I. *PAM Application Notes* **1**, 11-14 (2008).
37. Bailleul, B., Cardol, P., Breyton, C. & Finazzi, G. Electrochromism: a useful probe to study algal photosynthesis. *Photosynthesis Research* **106**, 179-189 (2010).

6. Supplementary Materials

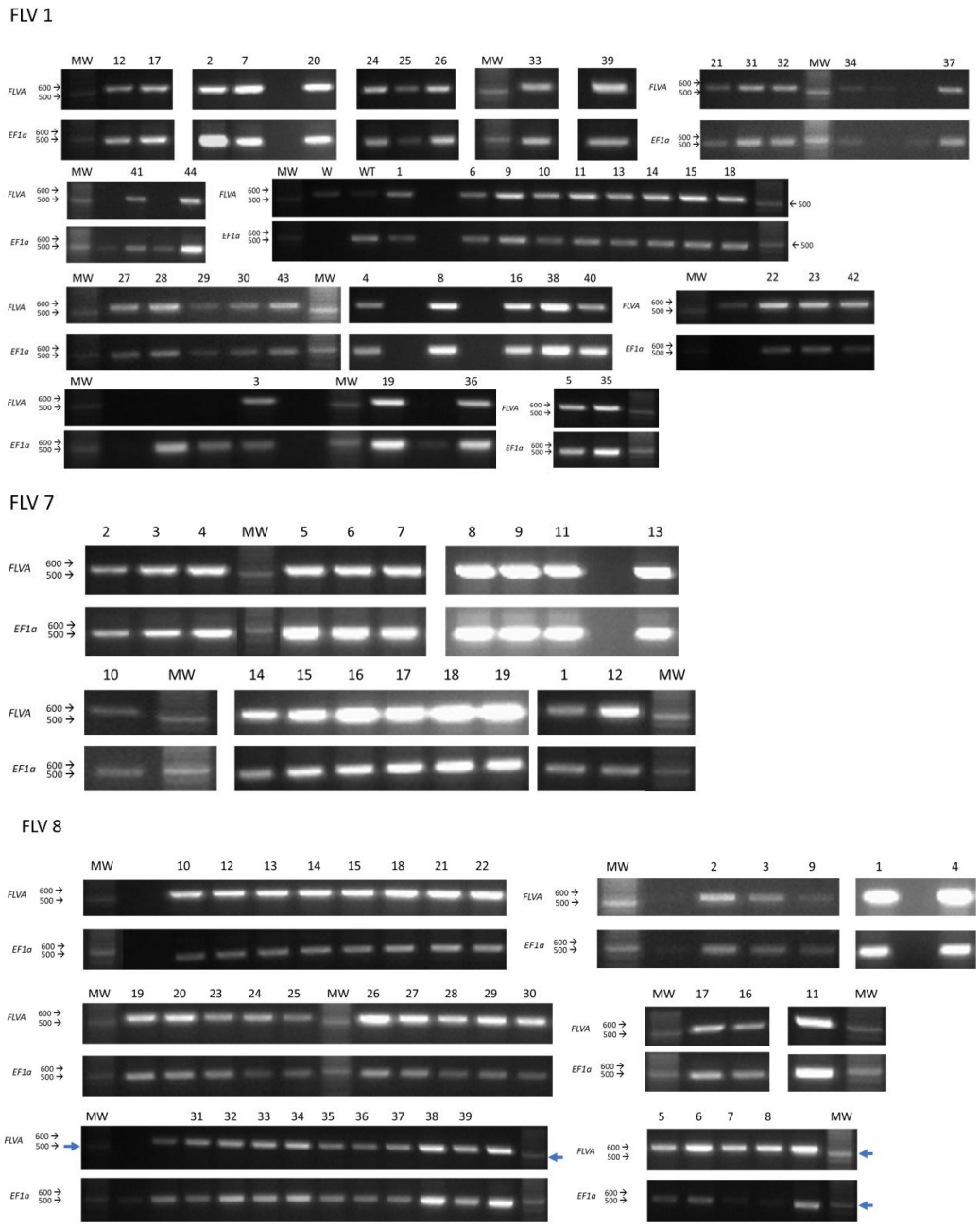

Fig. S1 – Agarose gel electrophoresis of the PCR performed on the gDNA extracted from each FLV *N. tabacum* line. All plants resulted positive for the presence of the transgene.

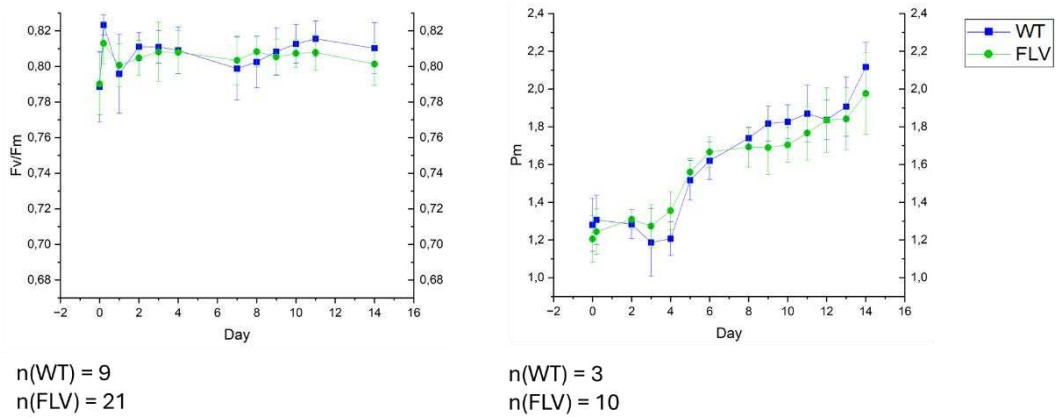

Fig. S2 - Daily Fv/Fm and Pm values of plants grown in control conditions. Data are presented as mean ± *s.d.*

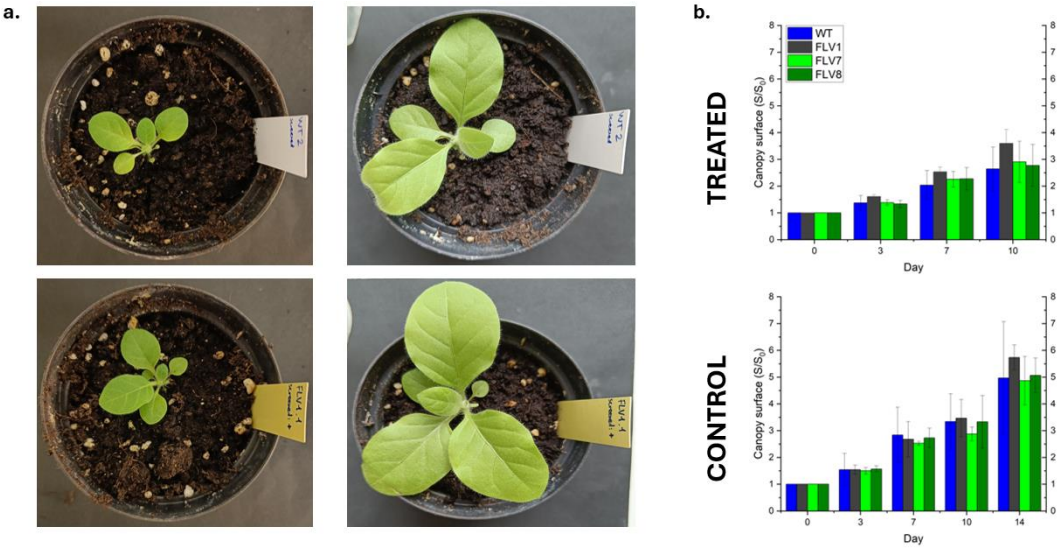

Fig. S3 - a) Comparison between day 0 and day 14 of a WT (upper half) and a FLV (lower half) plant, both grown under fluctuating light. Despite having the same number of leaves and having no difference at day 0, the FLV plant at day 14 shows a more developed canopy. b) Graph showing the canopy surface growth trend of WT plants along that of all three FLV lines, shown independently, normalized ad time 0 (before the start of the experiment).

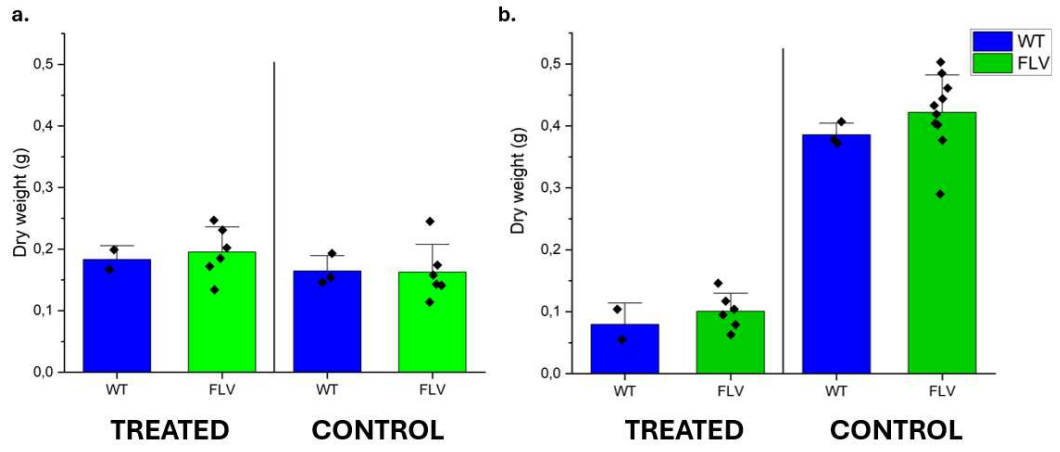

Fig. S4 – a) Dry weight data of the second repetition of the experiment. b) Dry weight data of the third repetition of the experiment, performed with different soil.

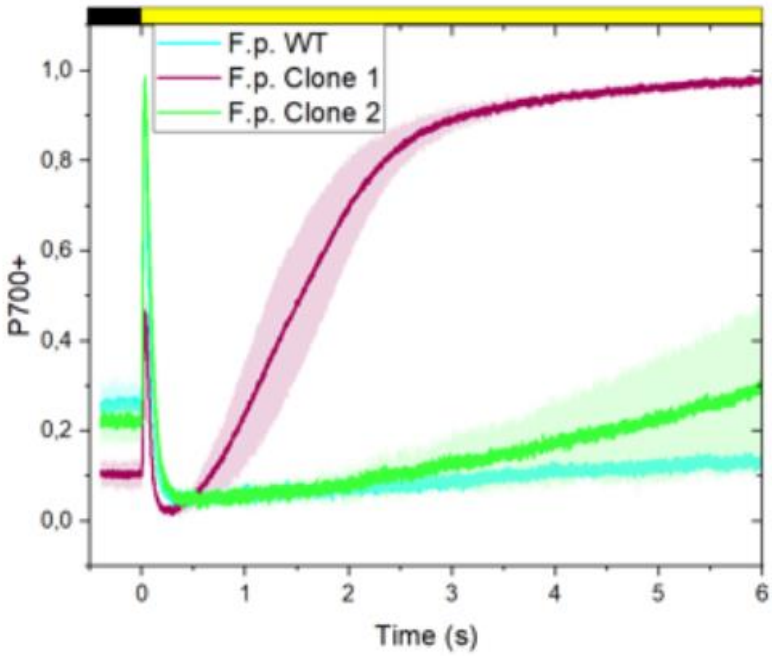

Fig. S5 – P700 redox kinetics of *Solanum lycopersicum* plants during a dark-to-light transition measured by Dr. Andrea Sabia. When FLVs are fully functional the SP-induced oxidation, and subsequent reduction, of P700 RCs is followed by a slower re-oxidation that is not seen in WT plants or in plants that do not fully express FLVs. Each line is the average value of the measurements performed on 3 independent leaves, standard deviation is reported as shadow around the lines.